Applied Energy 200 (2017) 1–18

Contents lists available at ScienceDirect

Applied Energy

journal homepage: www.elsevier.com/locate/apenergy

Economic dispatch of a single micro-gas turbine under CHP operation

Johannes F. Rist [a,1], Miguel F. Dias [b,1], Michael Palman [c], Daniel Zelazo [c,*], Beni Cukurel [c]

[a] Department of Mechanical Engineering, Technical University of Munich, Germany
[b] Department of Aerospace Engineering, Instituto Superior Técnico, Lisbon, Portugal
[c] Faculty of Aerospace Engineering, Technion - Israel Institute of Technology, Haifa, Israel

HIGHLIGHTS

- Economic dispatch of a micro gas turbine is considered for smart grid integration.
- A detailed thermodynamic cycle analysis is conducted for variable load CHP operation.
- Benefits are shown for case studies with real demand profiles and energy tariffs.
- Optimal unit schedule can be electricity, heat, revenue or maintenance-cost driven.

ARTICLE INFO

Article history:
Received 4 January 2017
Received in revised form 29 March 2017
Accepted 4 May 2017
Available online 11 May 2017

Keywords:
Micro gas turbines
Combined Heat and Power (CHP)
Polygeneration
Economic dispatch
Microgrids

ABSTRACT

This work considers the economic dispatch of a single micro-gas turbine under combined heat and power (CHP) operation. A detailed thermodynamic cycle analysis is conducted on a representative micro-gas turbine unit with non-constant component efficiencies and recuperator bypass. Based on partial and full load configurations, an accurate optimization model is developed for solving the economic dispatch problem of integrating the turbine into the grid. The financial benefit and viability of this approach is then examined on four detailed scenarios using real data on energy demand profiles and electricity tariffs. The analysis considers the optimal operation in a large hotel, a full-service restaurant, a small hotel, and a residential neighborhood during various seasons. The optimal schedule follows four fundamental economic drivers which are electricity, heat, revenue, and maintenance-cost driven.

1. Introduction

Presently, all business models (POLES, IEA, World Bank) forecast a drastic increase in the global demand for energy supply, where predictions reflect double the primary energy consumption from 2000 to 2020 [1]. More recent studies commissioned by the European Union, the U.S. Energy Information Administration (EIA), and the World Bank, all present similar projections of electricity demand increase by roughly 100% from 2000 to 2050 [2–4].

In order to satisfy this ever-growing electricity demand, the choice of fuel is among the challenges of economic policy. This choice is significantly dependent on national resources and long-term political interests. Although there exist variations in fuel type distribution between different countries [2], in an aggregate sense, it is expected that the relative shares of coal and nuclear are to decrease [4]. Charting the predictions of net electricity generation (in TWh) over the course of 50 years (until 2050), Fig. 1 presents the evolution of the dependency to various fuel sources. According to this EU energy market simulation, the future demand for power generation will be exceedingly accommodated by the renewable energy sources, as well as natural gas.

The issue of renewable energy, in particular solar and wind power, presents a specific challenge to the grid infrastructure. As their capacity is not always available, electricity generation becomes highly dependent on the time of day, the seasons, and the weather. The fluctuations in generation require more re-dispatches by grid operators, and therefore, the renewables alone cannot dominate the future generation infrastructure. Along these lines, the European Union's electricity generation from natural gas has tripled from the 1990s to early 2000s [5]. This trend of continued introduction of natural gas is foreseen in most industrialized countries.

The largest increase in the use of natural gas for power generation will primarily be accommodated by the introduction of

* Corresponding author.
E-mail addresses: johannes.rist@tum.de (J.F. Rist), miguel.f.dias@ist.utl.pt (M.F. Dias), p.michael@campus.technion.ac.il (M. Palman), dzelazo@technion.ac.il (D. Zelazo), beni@cukurel.org (B. Cukurel).

[1] The work was conducted during an internship at the Faculty of Aerospace Engineering, Technion - Israel Institute of Technology, Haifa, Israel.

http://dx.doi.org/10.1016/j.apenergy.2017.05.064
0306-2619/

Nomenclature

Abbreviations

CCHP	Combined Cooling, Heating and Power
CHP	Combined Heating and Power
COP	Coefficient of Performance
DAG	Directed Acyclic Graph
FAR	Fuel to Air Ratio
FC	Fixed Cost
FPE	Fixed Price of Energy
GT	Gas Turbine
HRU	Heat Recovery Unit
MGT	Micro Gas Turbine
PDC	Peak Demand Charging
ToU	Time-of-Use Energy Rate
UT	Utility
WP	Working Parameter

Economic dispatch nomenclature

ΔT	step size
$C_{GT}()$	fuel cost function
$C^P_{UT}(), C^H_{UT}()$	utility power and heat cost functions
$f_{GT}()$	turbine dynamics
$P(t), H(t)$	nominal power and heat demand
p_i, h_j	turbine speed and bypass valve position
$u_{GT}(t)$	turbine control variable at time t
$x_{GT}(t)$	turbine state at time t
$x^P_{UT}(t), x^H_{UT}(t)$	power and heat purchased from utility

Gas turbine nomenclature

$(\cdot)_{0i}$	stagnation conditions at station i
$(\cdot)_2$	compressor inlet station
$(\cdot)_{31}$	combustor inlet station
$(\cdot)_3$	recuperator cold inlet station
$(\cdot)_4$	turbine inlet station
$(\cdot)_{51}$	recuperator hot outlet station
$(\cdot)_5$	recuperator hot inlet station
$(\cdot)_6$	heat recovery unit inlet station
$(\cdot)_7$	heat recovery unit outlet station
$(\cdot)_{air}$	air parameter
$(\cdot)_b$	combustor parameter
$(\cdot)_{corr}$	corrected parameter
$(\cdot)_c$	compressor parameter
$(\cdot)_{dp}$	design point parameter
$(\cdot)_{el}$	electrical parameter
$(\cdot)_f$	fuel parameter
$(\cdot)_{HRU}$	HRU parameter
$(\cdot)_{max}$	maximal possible parameter
$(\cdot)_m$	mechanical parameter
$(\cdot)_{rec}$	recuperator parameter
$(\cdot)_{ref}$	reference conditions
$(\cdot)_s$	isentropic ideal process
$(\cdot)_t$	turbine parameter
β	HRU bypass valve position
$\dot{m}$	mass flow
$\dot{Q}_r$	specific fuel energy
η	efficiency
γ_c	heat capacity ratio - cold flow
γ_h	heat capacity ratio - hot flow
Ω	combustor loading parameter
ζ	bypass ratio
C	heat capacity
C_p	heat capacity at constant pressure
h	enthalpy
N	rotational speed
P	pressure
P_l	part load factor
$P_{compressor}$	compressor power
P_{gen}	generator power
P_{heat}	heating power
q	heat transfer rate
T	temperature

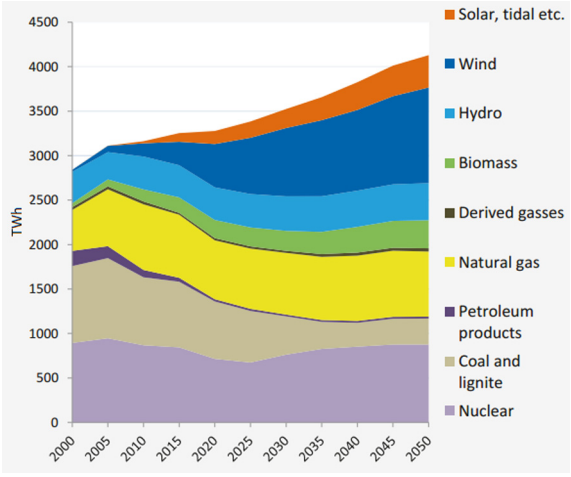

Fig. 1. Trends in electricity generation for the European Union (reproduced from [4]).

combined cycle systems, where the local consumers become the provider for their electricity, hot water, heat, and chill production [5–7]. The technological attractiveness of combined cooling, heat, and power (CCHP) units was the focus of several recent scientific studies [8–10]. Among the available options for CCHP production (such as internal-combustion, piston-steam, and stirling engines, as well as hydrogen fuel cells, combined solar plants, and steam-turbines), micro-gas turbines offer many advantages for small-scale generation. These include high power-to-weight ratio, relative size (low terrain footprint), reliability (smaller number of moving parts), lower noise and vibrations, multi-fuel capability, and lower greenhouse gas emissions [11–13]. Due to their relative low thermal and mechanical inertia, micro gas turbine units are agile and flexible, capable of short start-up times [14], along with rapid operational transitions between partial and full-load [11–13]. Furthermore, polygeneration systems that incorporate MGTs can theoretically achieve thermal efficiencies of above 85% [7].

This has motivated scientific efforts invested in determining the economically favorable conditions towards the smart grid integration of MGT powered CCHP units [15–20]. In these studies, the MGT model is often generic with fixed component and cycle efficiencies [15–18]. Furthermore, even when more refined models are considered [19,20], the thermo-economic analysis is either absent [20] or lacks realistic heat/power demand profiles and the associated variable pricing of electricity [15–19]. This level of abstraction is only sufficient to provide a first-pass estimate on whether a MGT may be suitable as a base load CCHP unit.

An economic dispatch solution of the MGT inherently requires a realistic CCHP system model (including part load operation) and actual consumer demand with utility pricing. In this direction, there remains the need of a focused research effort towards optimally integrating a realistic micro-gas turbine that considers variable component efficiencies, realistic heat and power demand profiles with actual electricity tariffs. Therefore, the motivation of this work is to determine the optimal schedule and commitment level of a micro gas turbine in a smart-grid scenario where power and heat demands can be in-part mitigated locally. The main contributions are:

- **Modeling of a micro gas turbine** - A detailed thermodynamic cycle analysis is conducted on a representative MGT unit with non-constant component efficiencies and recuperator bypass. This model provides a detailed MGT performance characterization in a range of operational conditions.
- **Economic dispatch of an MGT** - An optimization model based on the dynamic programming approach for economic dispatch is developed for the operation of an MGT.
- **Case studies** - Four detailed case study scenarios are provided to demonstrate the advantage of using MGTs for CHP generation. The economic dispatch problem for typical 24-h days (winter, summer, spring) are solved for a large hotel, small hotel, full service restaurant, and residential neighborhood.

In addition to an economic analysis of integrating the MGT into the grid, the case studies also revealed that the MGT operates under four distinct economic driving modes: *electricity driven*, *heat driven*, *revenue driven*, and *maintenance-cost driven*. Each mode describes the economically optimal way to operate for a given demand profile, fuel costs, and the tariffs. This leads to important insights into the economic dispatch solution and a high-level understanding of how the MGT can best be integrated into the grid.

The organization of this paper is as follows. In Section 2, the detailed thermodynamic model of the polygeneration suitable micro gas turbine unit is presented. Section 3 describes the integration of the MGT model in an economic dispatch framework. Case studies demonstrating the advantage of using MGT as a CHP unit in a smart-grid setting are presented in Section 4. Finally, some concluding remarks are offered in Section 5.

2. Gas-turbine modeling

Micro gas turbines are exceptionally suitable to meet the on-site needs of distributed power generation. However, a proper thermodynamic analysis coupled with thermo-economic investigation must be carried out to gain essential information on the various available cycle solutions [21]. Beyond the general trends, to provide valid estimations of economic value, the power distribution scenarios must include realistic energy demand/cost models, as well as an accurate component level characterization of the MGT.

To this end, most previous efforts related to the economic dispatch problem simulated the MGT as a dynamic system using the governor model [22–25]. This approach can capture the electro-mechanical response of a generic turbine coupled with a generalized controller, while disregarding the energy conservation laws of individual components (compressor-turbine coupling, combustor performance, and mechanical losses), which mainly hinders part load performance prediction. Addressing this issue to a limited extent, there has been steady reduced models, which are geared towards capturing the nominal and part load trends by empirical fits to the publicly available manufacturer datasheets [26]. Moreover, the part load behavior was linearized by approximations based on turbomacinery physics [27]. This formulation is particularly useful in concept phase of energy planning in decentralized systems. Increasing in complexity, dynamic characteristics of the compressor and turbine were represented by fully nonlinear analytical expressions, instead of the more typical polynomial approximations [28]. Nevertheless, the accuracy of this general approach is limited by the mathematical abstraction of the component maps.

In parallel, there has been significant efforts invested into treating the entire system as a black box (absent of physical equations). This led to the implementation of an artificial neural network approach in the context of micro gas turbine driven combined heat and power generation [29]. Relations between the inputs and outputs are built up during the training process, and based on the sensitivity analysis, the preferable set of parameters are determined. The basic requirement of this methodology is a running available MGT, where experimental training points can be generated.

Nevertheless, towards a more accurate description of MGT performance in nominal and off-design conditions, the current state-of-the-art in the turbomachinery community is still component based models with varying degree of complexity, [30–33]. In the scope of the current work, we also implemented a component-based gas turbine model that resolves the steady-state performance of a realistic CHP unit, allowing accurate performance optimization of its commitment.

2.1. The micro-gas turbine for polygeneration

There exist a broad range of studies on advanced cycle design and analysis for various applications. Focusing on the balance between opposing trends associated with capital (fixed) and variable costs of different MGT cycles, it has been shown that recuperated cycles are the preferable means of generation for units smaller than $100kW_{el}$ [21]. At these scales, the intercooled recuperative cycles are relatively more efficient, however their market penetration is vastly hindered by the increased capital and electricity production costs. Therefore, due to its compromise in efficiency with respect to capital cost, reduced mechanical complexity, and imminent applicability, a small single-spool gas turbine engine is being considered in the recuperated cycle. The nominal power output of the discussed unit is $100kW_{el}$. The proposed micro-gas turbine model features compact and reliable design that requires low maintenance and operates at competitive efficiency and scale with other energy production technologies such as small reciprocating engines.

Comparative CHP gas turbine units exist in the product portfolio of various companies. For example, Capstone C65, Ingersoll Rand PowerWorks 70, Ansaldo Energia (formerly Turbec) AE-T100, Dürr Cleantechnology Compact Power System, and Elliot TA100 all operate in this power range. From publicly available data [34–39], operational parameters of these commercial products are summarized in Table 1.

However, most consumers of these products are rarely interested in operating the unit solely at its design point and typically would like to vary the commitment level based on demand and cost of alternate available energy resources. Therefore, the design point information provided by the manufacturer is insufficient to properly assess the economic value, as the product ideally should also operate under off-design (part load) conditions. Hence, a more detailed model of a relevant micro-gas turbine is required to adequately resolve the performance in the entire operational range.

Based on the engine architecture relevant to the industry, the MGT unit we consider consists of a single stage centrifugal compressor, a can-type combustor, a single stage turbine, and a recuperator. In order to accommodate the changing ratio between

Table 1
Design output parameters of reference MGT units operated in CHP.

	Power (kW)	Heat (kW)	Electrical efficiency (%)	Cycle efficiency (%)
Capstone C65	65	126	29	up to 90
I-R PW70	70	106	28	70
AE-T100	100	200	30	90
Durr CPS	100	210–520	30	up to 98
Elliot TA100	100	165	29	75

power and heat generation demand, the recuperator is equipped with a controllable valve which alters the amount of exhaust gasses bypassing the heat exchanger. The schematic of the discussed CHP unit cycle is presented in Fig. 2.

The mechanical energy of the shaft is to be extracted by an asynchronous generator, connected to the grid via a voltage and frequency conditioning circuit that includes a rectifier, a DC boost chopper, an inverter bridge, and a filter. Depending upon the geographic location, the output of the power electronics is 400VAC/50 Hz or 480VAC/60 Hz. Moreover, the system is to include a heat recovery unit (HRU), which is meant to supply the required heat/chill production. However, due to significant differences amongst various applications, the exact mechanical to electrical energy conversion process and the exhaust heat utilization method (via boiler or adsorption chiller) are not modeled in the scope of this investigation.

2.2. Thermodynamic equations

Both design and off-design operating parameters of the CHP unit model can be derived from thermodynamic equations that describe the performance of individual non-ideal MGT components. The following sections describe the process towards performance evaluation of each element. For proprietary reasons, component characteristics are often not disclosed. Hence, performance parameters of a typical small gas-turbine engine are used throughout the study [40].

2.2.1. Compressor

In general, the behavior of the compressor in the MGT is described by a map which charts the operational envelope in terms of pressure ratio (PR), corrected mass flow rate ($\dot{m}_{corr}$), corrected rotational speed (N_{corr}), and efficiency (η_C), as depicted in Fig. 3 (a). The non-dimensional numbers are defined as,

$$\dot{m}_{corr} = \frac{\dot{m}\sqrt{T/T_{ref}}}{P/P_{ref}} \tag{1}$$

$$N_{corr} = \frac{N}{\sqrt{T/T_{ref}}}, \tag{2}$$

where N is the shaft rotational speed, $\dot{m}$ is the mass flow rate through the engine, T is the inlet temperature, P the inlet pressure,

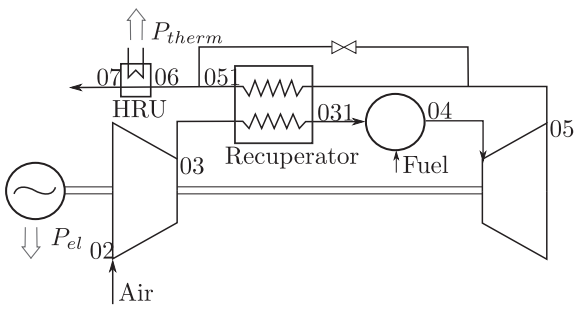

Fig. 2. Thermodynamic cycle of a recuperated gas turbine with a heat recovery unit.

and T_{ref}, P_{ref} are standard temperature and pressure reference conditions.

The various speed lines span across the pressure range at their respective efficiency islands. However, in parts of the map, these speed lines can be horizontal or vertical, and render several possible operating points for a given pressure ratio or mass flow requirement. To resolve this ambiguity, auxiliary coordinates (typically known as "beta lines") are introduced. Once the appropriate operating point has been selected on the map, the compressor performance is linked to the thermodynamic cycle by

$$\eta_c = \frac{h_{03s} - h_{02}}{h_{03} - h_{02}} \tag{3}$$

$$T_{03} = T_{02}\left(\frac{1}{\eta_c}\left(\left(\frac{P_{03}}{P_{02}}\right)^{\frac{\gamma_c - 1}{\gamma_c}} - 1\right) + 1\right), \tag{4}$$

which relate the non-ideal work addition to the efficiency and the resultant pressure ratio respectively. The subscripts in the equations refer to the station numbers labeled in Fig. 2, and the subscript s denotes the state hypothetically achieved through an isentropic ideal process.

2.2.2. Recuperator

After the pressure rise in the compressor, the temperature of the outgoing flow is further raised by the energy recovered through the recuperator. The efficiency of this process is characterized by

$$\eta_{rec} = \frac{q}{q_{max}} = \begin{cases} \frac{c_{p,05}\dot{m}_5(T_{05} - T_{051})}{c_{p,03}\dot{m}_3(T_{05} - T_{03})}, & c_{p,03}\dot{m}_3 < c_{p,05}\dot{m}_5 \\ \frac{(T_{05} - T_{051})}{(T_{05} - T_{03})}, & c_{p,05}\dot{m}_5 < c_{p,03}\dot{m}_3 \end{cases}, \tag{5}$$

which captures the non-ideal heat transfer between the relatively hot and cold gas paths. When electrical power output is required from the unit, the performance of the recuperator highly influences the fuel consumption of the MGT. In contrast, to accommodate high heat or chill demand, the recuperator bypass valve is regulated to retain the exhaust gas temperature. In the scope of this study, the efficiency values are taken from a recuperator of appropriate size [41], the performance data for which is reproduced in Fig. 4.

2.2.3. Combustor

The thermal energy addition of the cycle takes place in the can type combustor, characterized by

$$(\dot{m}_{air} + \dot{m}_f)h_{04} - \dot{m}_{air}h_{031} = \dot{m}_f\dot{Q}_r\eta_b \tag{6}$$

$$\eta_b = 1 - (1 - \eta_{b,dp})(\Omega/\Omega_{dp})^{P_l} \tag{7}$$

$$\Omega = \frac{\dot{m}_{air}}{P_{03}^{1.8} \cdot exp(T_{03}/300)}, \tag{8}$$

where $\eta_{b,dp} = 0.98$ and $\Omega_{dp} = 0.0160, P_l = 1.6$ and $Q_r = 49,736,500$ J/kg. Eq. (6) describes the conservation of energy between the incoming air, the caloric value of the fuel burned, and the outgoing combustion products. To calculate the efficiency of this process, an empirical model is introduced in (7). Based on known design point conditions, the off-design efficiency is modeled with reference to combustor loading parameter, (8).

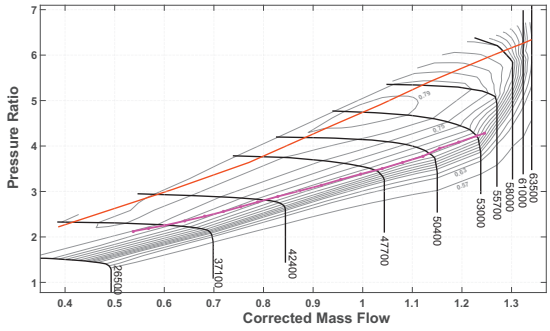

(a) Compressor map: pressure ratio (PR) vs corrected mass flow.

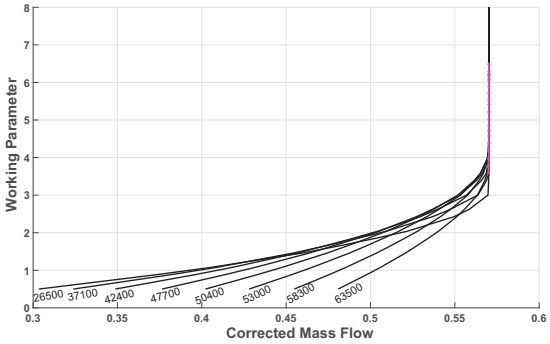

(b) Turbine map 1: working parameter (WP) vs corrected mass flow.

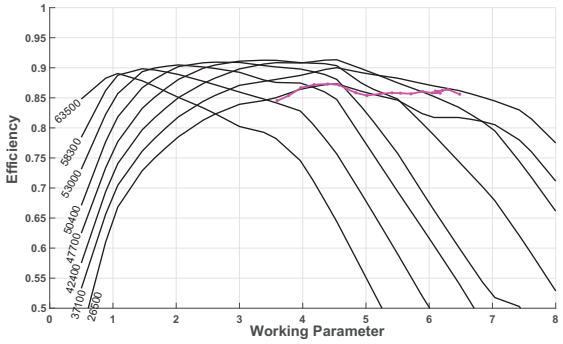

(c) Turbine map 2: working parameter (WP) vs Turbine Efficiency.

Fig. 3. Compressor and turbine maps with an exemplary operating line.

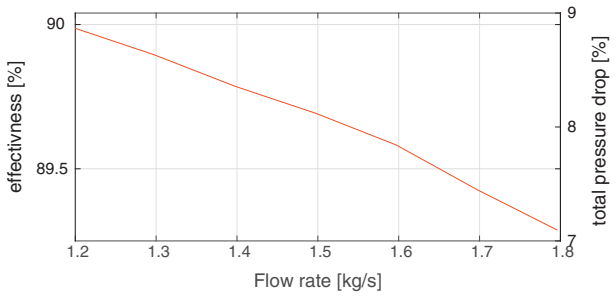

Fig. 4. Heat exchanger performance.

2.2.4. Turbine

The thermal to mechanical energy conversion takes place in the turbine. Two charts are required to describe the turbine operating envelope - the first represents the behavior of the component in terms of the working parameter (WP) as a function of corrected mass flow and corrected rotation speed (Fig. 3(b)), and the second relates to the efficiency of the conversion process (Fig. 3(c)). For convenience, the definition of the working parameter is provided below,

$$WP = 0.0239 \frac{T_{04} - T_{05}}{T_{04}} \cdot C_p(T_{04}). \tag{9}$$

Portraying the non-ideal nature of the expansion process, the following relations can be written

$$\eta_t = \frac{h_{04} - h_{04}}{h_{04} - h_{05s}} \tag{10}$$

$$\frac{T_{04} - T_{05}}{T_{04}} = \eta_t \left(1 - \left(\frac{P_{04}}{P_{05}} \right)^{-\frac{\gamma_h - 1}{\gamma_h}} \right) \tag{11}$$

In the following, the energy extracted by the turbine with respect to the energy consumed by the compressor and the generated electrical power are balanced as

$$\overbrace{\dot{m}_{air}(h_{03} - h_{02})}^{P_{compressor}} + P_{gen} = \eta_m (\dot{m}_{air} + \dot{m}_f)(h_{04} - h_{05}). \tag{12}$$

2.2.5. Heat recovery unit

Passing through the hot side of the recuperator, the last station of this cycle is the Heat Recovery Unit (HRU). Providing a heat (or indirectly a chill) source for the consumer, this component extracts heat from the exhaust gasses. After the flow of recuperator exit and the bypass duct undergo flow mixing, HRU essentially acts an additional heat exchanger, and therefore its performance model is synonymous with the recuperator,

$$h_{06} = h_{051} \cdot (1 - \beta) + h_{05} \cdot \beta \tag{13}$$

$$P_{heat} = \eta_{HRU} \dot{m}_5 \cdot (h_{06} - h_{07}). \tag{14}$$

The outlet temperature after the HRU is typically higher than 100 °C [42], and therefore the outlet enthalpy h_{07} is calculated for this constant value.In the cooling mode of operation, the absorption chiller is directly driven by the waste heat extracted from the heat recovery unit. Detailed modeling of absorption chiller is highly complex

[43] and beyond the scope of this work. Therefore, an absorption chiller, with constant performance, is considered. The efficiency of this process is described by the coefficient of performance (COP),

$$COP = \frac{\text{Cooling Power}}{\text{Heating Power}} \tag{15}$$

which is typically assumed to be 0.7 for single-stage units [44,45]. Thereby, with the COP formulation, the demand for chill is related with the demand for waste heat.

2.3. Numerical modeling of micro-gas turbine

Solving the equations developed in Section 2.2 can be used to generate the steady-state relationship between the MGT shaft speed, bypass valve position, and fuel consumption. This directly relates to the cost of locally producing electricity and heat at a desired level which can be used to optimize its operation when integrated into the power grid.Although the thermodynamic behavior of various MGT components are well defined, the solution methodology for finding their steady-state relations can be non-trivial. In the scope of this work, an approach based on NASA's DYNGEN algorithm [30] is used; the flow chart is presented in Fig. 5. On a similar scale MGT, the high level of accuracy of this technique was prior demonstrated in [46]. For a given shaft rotational speed and bypass valve position, the location on the compressor beta line is initially assumed. Then, the mass flow, pressure ratio and efficiency are extracted from the compressor map, setting T_{03}. The temperature downstream of the combustor (T_{04}) and the recuperator (T_{031}) are guessed sequentially to initiate the two inner-loops of the compressor-turbine matching. The required fuel flow, which matches the prescribed T_{04}, is subsequently calculated to find T_{05}. These values are used to extrapolate mass flow, pressure ratio and efficiency from the turbine maps. At first, the mass flow through the turbine is calculated and T_{031} is updated until convergence. In following, the fuel mass flow is iterated upon. Finally, the initial beta line guess is revised by the calculation of the HRU exhaust pressure. When the algorithm fully converges, a steady state solution is reached, which relates the fuel mass flow rate, electrical power, and heat output to the shaft rotational speed and bypass valve position.

2.4. Cycle parameters for operational optimization

In order to optimize the MGT cycle during its operation, two input parameters (shaft speed and bypass valve position) are selected and simulated to yield a number of solution states (electrical power, heat output, and fuel mass flow). For this study, we considered 9 discrete speed levels (from 66% to 100% of rated rpm) and 5 discrete bypass settings (from 0% to 80%). The discrete parameter maps of these steady-state relations are presented in Fig. 6.

The thermodynamic performance of the MGT is characterized in electrical power and heat output domains ranging between 30–110 kW_{el} and 57–452 kW respectively; see Figs. 6(a)–(c). For a closed bypass valve, while the heat to power output ratio is between 1.4–1.8, this range reaches values of 4.5–7.5 at maximal 80% bypassing. Moreover, providing a measure for CHP unit performance, the heat and electricity generation efficiencies are represented in Fig. 6(d) and (e) respectively. For a fixed electrical output, when the recuperator bypass valve is opened, the heat output expectedly increases, along with the heat generation efficiency. Although the rotational speed of the shaft is retained throughout this process, due to the increase in fuel mass flow rate that satisfies the energy balance, the electrical efficiency drops. Across the operating conditions in the range of 0–80% bypassing, the electricity and heat generation efficiencies vary between 41–9% and 52–71% respectively. These values are consistent with the units existing in the market - see Table 1.

3. Economic dispatch for micro-gas turbines

The detailed modeling of the micro-gas turbine allows for realistically considering its integration into a power generation system. In this direction, we apply the model developed in Section 2 to an optimal economic dispatch framework. While there are many approaches for solving the economic dispatch problem [47–52], the discretized model of the MGT makes it amenable to a dynamic programming-based strategy [53–55]. Moreover, as we are focusing on the understanding of the economic feasibility and comparative advantage of an MGT, we are not concerned with real-time solutions. Therefore, for this study we employ a *shortest-path* solution method for the dynamic programming approach to economic dispatch [56–58]. The shortest-path modeling, which is reviewed in this section, is based on the previous work [59].

3.1. Optimization model for micro-gas turbines

The economic dispatch (ED) problem is the short-term optimal determination of generation unit outputs aimed at satisfying the system load while minimizing the overall cost. In this work, the operation of a micro-gas turbine as a CHP unit is considered, and thus the ED problem is to determine optimal schedules for both the power output and heat generation of the MGT that minimizes the overall cost to the user. This includes costs incurred from the operation of the MGT (mostly attributed to fuel), in addition to the cost of purchasing power and heat from the utility in the event that the turbine is not economically feasible to operate, or when it can not completely satisfy the demands.

We denote by $x_{GT}(t)$ the MGT state corresponding to a given power and heat output level at time t. As discussed in Section 2.4 and summarized in Fig. 6, the generator power and heat output are directly related to the turbine speed and bypass valve setting. For generality, we assume the turbine can operate at s fixed speed levels - each speed level is denoted as p_i, for $i = 1, \ldots, s$. The amount of heat the turbine can output is a function of the bypass valve that takes a value between 0 (closed) and 1 (completely open). This is denoted by the variable h_j, for $j = 1, \ldots, v$ with $h_1 = 0$ and $h_v = 1$. Thus, the complete state of the turbine can be characterized by the pair $x_{GT}(t) = (p_i(t), h_j(t))$.

The MGT speed and valve setting can be mapped directly to the fuel mass flow, as shown in Fig. 6(a). Thus, the cost of operating the generator at a given state is a function of the cost of fuel and the function $C_{GT}(x_{GT}(t))$ is the fuel cost for operating the turbine at that level.

Similarly, the variables $x^p_{UT}(t)$ and $x^H_{UT}(t)$ denote the power and heat commitment purchased from the utility[2] at time t with cost functions $C^p_{UT}(x^p_{UT}(t))$ and $C^H_{UT}(x^H_{UT}(t))$ respectively. The ED cost function for a finite time horizon of T units can be expressed as

$$J(x_{GT}, x^p_{UT}, x^H_{UT}) = \sum_{t=1}^{T} \Big(C_{GT}(x_{GT}(t)) + C^P_{UT}(x^p_{UT}(t)) + C^H_{UT}(x^H_{UT}(t)) \Big). \tag{16}$$

The minimization of the cost function (16) is subject to several restrictions capturing both the power and heat balance of the system, and the operational constraints of the generator. The energy balance equations are the thermodynamic and power restrictions of the microgrid operation. We denote the nominal demand for

[2] Heat is not directly sold by the utility, but can be modeled as an additional fuel or electricity cost. This is discussed in more detail in Section 4.1.2.

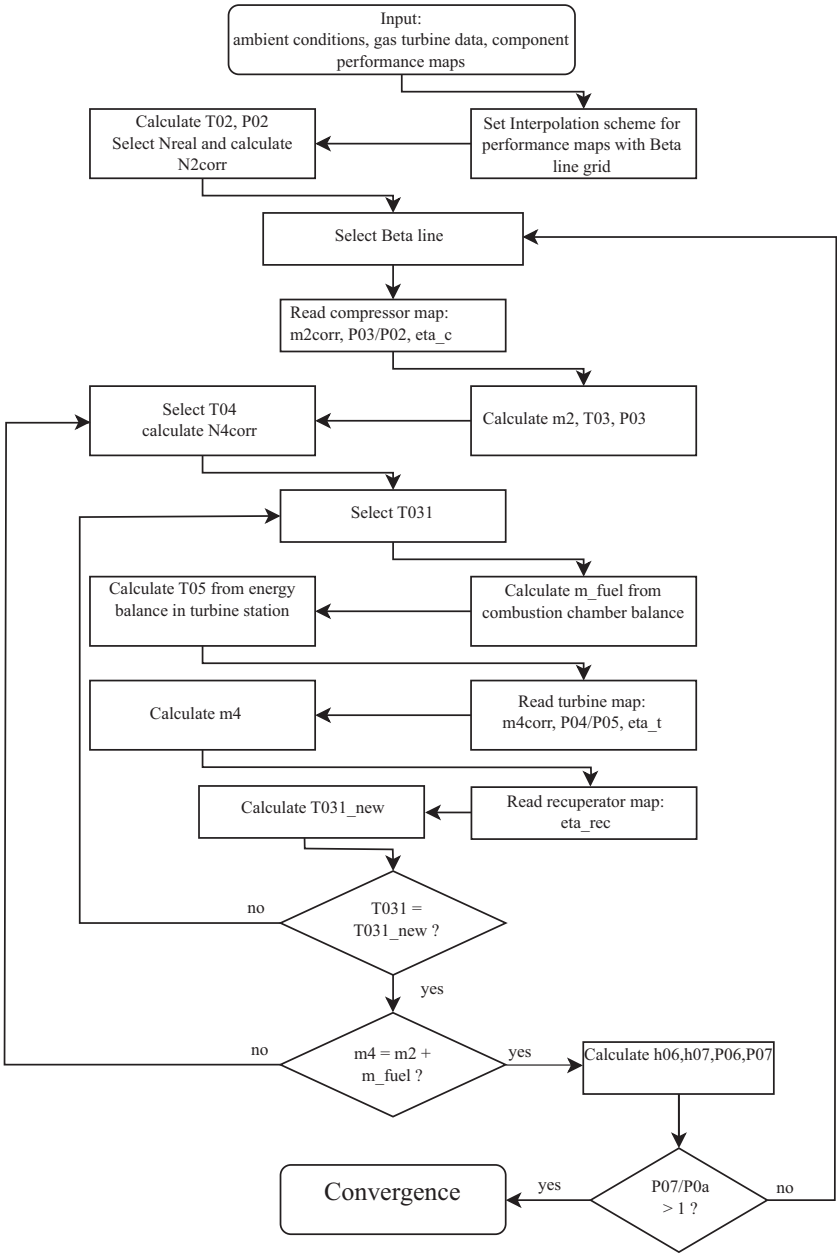

Fig. 5. Numerical simulation model flowchart of the recuperated MGT.

power and heat at time t with the variables $P(t)$ and $H(t)$. For the turbine state $x_{GT}(t)$, there is a corresponding power and heat output, denoted by $P_{GT}(x_{GT}(t))$ and $H_{GT}(x_{GT}(t))$ respectively (Figs. 6(b) and (c)). Thus, the energy balance can be expressed as

$$P_{GT}(x_{GT}(t)) + x^{P}_{UT}(t) = P(t), \quad t = 1, \ldots T, \tag{17}$$

$$H_{GT}(x_{GT}(t)) + x^{H}_{UT}(t) = H(t), \quad t = 1, \ldots, T. \tag{18}$$

In the absence of any additional constraints, the ED problem aims to minimize (16) subject to the energy balance constraints (17) and (18).

While one may consider purchasing power and heat from the utility in an instantaneous manner, extracting heat and power from the MGT implicitly induces dynamics, which we develop here. Recalling that the time constant corresponding to changes in the MGT state are fast relative to the operating horizon, this economic dispatch problem considers transition from one MGT state to another via steady-state operational behavior only.

In this direction, we introduce a control variable for the MGT, denoted $u_{GT}(t)$, which is used to determine how the turbine should change states at each time-step. For any turbine state $x_{GT}(t)$, there may be a multitude of allowable states the turbine can transition to, and the control signal $u_{GT}(t)$ is used to abstractly represent this.This leads to a discrete-time dynamical system, represented below as,

$$x_{GT}(t + c\Delta T) = f_{GT}(x_{GT}(t), u_{GT}(t)), \tag{19}$$

where a fixed step-size of ΔT seconds is assumed. As we are concerned with only the steady-state operation, the step-size should be chosen to be faster than the transient dynamics, but short enough to capture the scheduling objective for the ED problem.

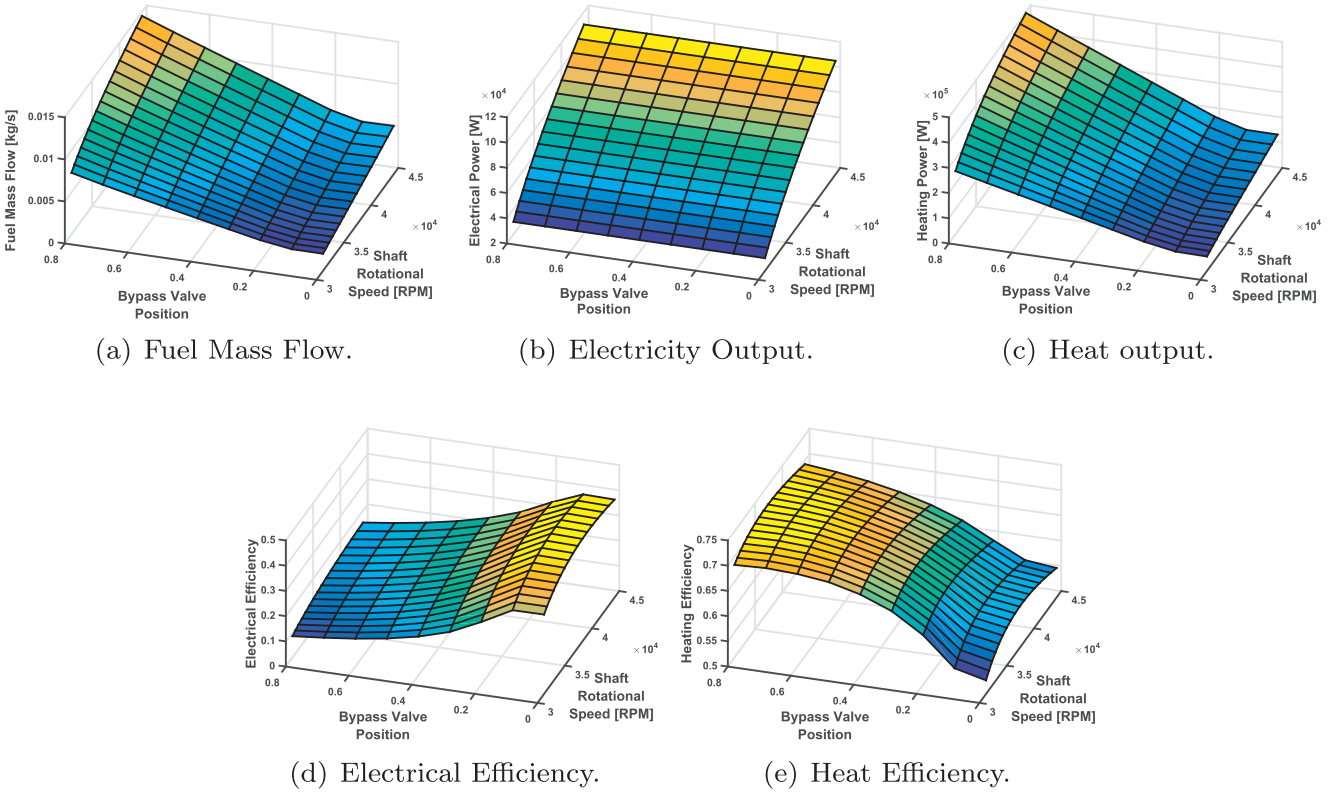

(a) Fuel Mass Flow. (b) Electricity Output. (c) Heat output.

(d) Electrical Efficiency. (e) Heat Efficiency.

Fig. 6. Solution grid over the states of the gas turbine model.

The constant c is used to emphasize that certain transitions may require multiple time-steps to complete.[3]

The form of the function f_{GT}, therefore, captures both the allowable state transitions of the MGT, and the number of time steps each transition requires. As shown in [59], dynamics expressed in this form can be represented by a state-transition diagram leading to a qualitative description of the dynamics (19). As an illustrative example, consider the steady-state operation of the turbine with bypass level fixed to h_1. The state-transition diagram representing allowable power level transitions is depicted in Fig. 7. It can be observed in this example that increasing the speed level requires two time-steps (i.e., $c = 2$), while decreasing requires a single time-step (i.e., $c = 1$). Furthermore, speed levels must be increased or decreased sequentially (for example, the generator can not transition from state (p_1, h_1) to (p_3, h_1) without passing through (p_2, h_1)). However, it is possible to change both the speed level and the bypass valve setting in the same time step, provided that the requirement of sequential speed changes are respected. Note that Fig. 7 represents only a portion of the complete state-transition diagram, which contains $p_s h_v$ possible states at each time step. The exact number of time steps required for changing states depends on the step-size ΔT. In this setting, the control variable $u_{GT}(t)$ represents the decision variable deciding which edge to take from a given state in the transition graph.

The MGT also requires special start-up and shut-down procedures. When the generator is in the 'off' state (corresponding to $x_{GT} = (0, 0)$), it must be ramped up to full power (i.e., p_s with any bypass valve setting). Furthermore, the transition from the 'off' state to the first online state takes T_{SU} minutes. Hence, if increasing the speed level takes two time-steps, the complete start-up procedure takes $SU_t = T_{SU}/\Delta T + 2\Delta T \cdot s$ time steps. Similarly, the generator can only be shut down from the state (p_1, h_1) and requires T_{sd} units of time to be completely off-line. Fig. 8 depicts the transition graph highlighting the beginning of a start-up procedure where T_{SU} corresponds to 4 time steps. We assume for this study a start-up time for the MGT of 2 min, and a shut-down time of 3 min [14]. Note that this formulation also implicitly includes other

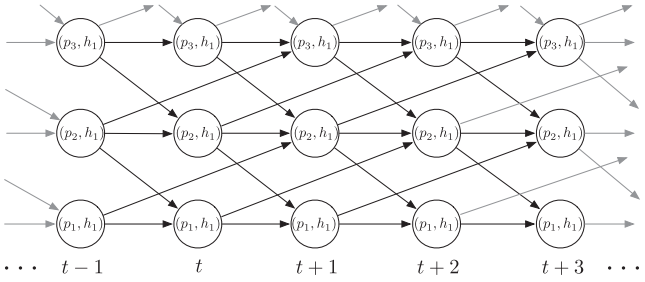

Fig. 7. A portion of the transition graph of MGT during online operation.

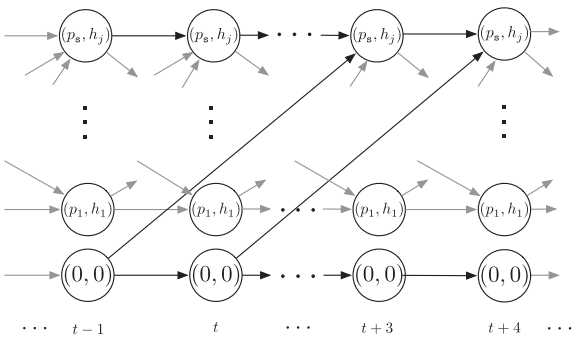

Fig. 8. Portion of the start-up transition diagram for MGT.

constraints such as ramp-rates of the MGT. A typical ramp-rate constraint is expressed as

$$DR \leqslant p_j(t+c\Delta T) - p_i(t) \leqslant UR,\ i,j \in \{1,\ldots,s\},$$

where DR and UR are the ramp-down and ramp-up rate limits, respectively. Thus, there can only be an edge connecting the states corresponding to power outputs $p_j(t+c\Delta T)$ and $p_i(t)$ if and only if they satisfy the above inequality.

Using this state-transition graph representation, it is possible to embed in the generation cost a *transition* cost that models the added cost for changing states. We assume that the generation cost, $C_{GT}(x_{GT}(t), u_{GT}(t))$, includes these transition costs. This allows to completely characterize the economic dispatch problem for operating the MGT in a smart-grid environment as the optimization problem

$$\begin{aligned}
\min_{x_{GT},u_{GT},x^P_{UT},x^H_{UT}} \quad & J(x_{GT},u_{GT},x^P_{UT},x^H_{UT}) \\
\text{subject to} \quad & x_{GT}(t+c\Delta T) = f_{GT}(x_{GT}(t),u_{GT}(t)), \\
& P_{GT}(x_{GT}(t)) + (x^P_{UT}(t) - P(t)) = 0, \\
& H_{GT}(x_{GT}(t)) + (x^H_{UT}(t) - H(t)) = 0, \\
& x_{GT}(t) \in \{(p_i(t),h_j(t)),\ i=1,\ldots,s, j=1,\ldots,v\} \\
& x^P_{UT}(t) \geqslant 0,\ x^H_{UT}(t) \geqslant 0,\ t=1,\ldots,T.
\end{aligned} \tag{20}$$

In the next subsection, solution methods for (20) will be discussed.

3.2. Solution methods - a shortest path approach

The general form of the optimization problem in (20) falls under the class of mixed-integer programming (MIP) and dynamic programming. The description of the dynamics using a state-transition graph allows for employing the shortest path algorithm to solve the problem [57,59]. As shown in Section 3.1, each node in the graph represents the operating state of the MGT (the state $x_{GT}(t)$) at a given time t, and the decision variable (i.e., the control $u_{GT}(t)$) is represented by the edges connecting nodes in the graph. Thus, if we operate for T units of time with time-steps of ΔT, the complete network must contain $p_s h_v T/\Delta T$ nodes. The edges of the graph are determined by the MGT discretized dynamics (19). Hence the graph can be constructed independently of the cost assignment. Furthermore, given that the graph evolves forward in time, it can be categorized as a *directed acyclic graph* (DAG), which leads to efficient shortest path algorithms [60,61].

The main challenge for employing the shortest path algorithm is to accurately map the cost functions, described on the nodes of the graph, to appropriate transition costs assigned to each edge. Furthermore, the cost structure must embed the enforcement of the energy balance constraints. In this direction, recall that the energy balance constraints (17) and (18) are always satisfied - power and heat is purchased from the utility whenever the MGT does not meet the demand. Thus, each generator state $x_{GT}(t)$ determines the amount of power and heat to be purchased from the utility explicitly (the costs $C^P_{UT}(x^P_{UT}(t))$ and $C^H_{UT}(x^H_{UT}(t))$). To compute the edge weight between adjacent nodes, we assume the cost to be the average cost between the adjacent edges. In this direction, we denote by $\overline{P}(t,t+c\Delta t)$ and $\overline{H}(t,t+c\Delta t)$ as the average power and heat demand over the time interval t and $t+c\Delta t$. The MGT cost associated with the edge is computed as

$$\overline{C}_{GT}(t,t+c\Delta T) = c\Delta T \frac{C_{GT}(x_{GT}(t)) + C_{GT}(x_{GT}(t+c\Delta T))}{2},$$

and the average power and heat supplied by the MGT is

$$\overline{P}_{GT}(t,t+c\Delta T) = c\Delta T \frac{P_{GT}(x_{GT}(t)) + P_{GT}(x_{GT}(t+c\Delta T))}{2}$$
$$\overline{H}_{GT}(t,t+c\Delta T) = c\Delta T \frac{H_{GT}(x_{GT}(t)) + H_{GT}(x_{GT}(t+c\Delta T))}{2}.$$

The cost of the power and heat purchased from the utility can then be computed as

$$\overline{C}^P_{UT}(t,t+c\Delta T) = c\Delta T C^P_{UT}\big(\overline{P}(t,t+c\Delta t) - \overline{P}_{GT}(t,t+c\Delta T)\big)$$
$$\overline{C}^H_{UT}(t,t+c\Delta T) = c\Delta T C^H_{UT}\big(\overline{H}(t,t+c\Delta t) - \overline{H}_{GT}(t,t+c\Delta T)\big).$$

Note that if $\overline{H}(t,t+c\Delta t) - \overline{H}_{GT}(t,t+c\Delta T) < 0$, the excess heat is dumped into the atmosphere and the cost is 0. In summary, the edge transition cost can be expressed as

$$\begin{aligned}
e(x_{GT}(t),x_{GT}(t+1)) = {} & \overline{C}_{GT}(t,t+c\Delta T) + \overline{C}^P_{UT}(t,t+c\Delta T) \\
& + \overline{C}^H_{UT}(t,t+c\Delta T).
\end{aligned} \tag{21}$$

In addition to the costs described above, there is a cost associated with the start-up and shut-down of the unit. Considering that the price of the gas turbine engine is roughly $75,000, and based on typical low cycle fatigue life of 10,000 cycles [62], it is possible to estimate the cost of each shutdown and startup as $3.75 each. During the startup and shutdown procedures, we assume the MGT is offline for the entire duration, and thus all electricity and heat much be purchased from the utility, contributing to the edge cost.

To complete the construction of the graph, artificial "start" and "end" nodes are added; these states are unrestricted and do not represent a constraint for the optimization. Thus, we allow the optimization to begin at any generator state without incurring a cost. The above modeling provides a methodical way to construct the directed acyclic graph. In this scenario, the shortest path solution would correspond precisely to the optimal operating schedule of the MGT.

4. Case studies

To demonstrate the benefit of integrating a single micro gas turbine into the electricity market, we provide four detailed case studies: a full-service restaurant, a large hotel, a residential building neighborhood and a small hotel. In the following, we present a detailed model of the demand profiles and electricity tariffs for each scenario. We then solve the economic dispatch problem for a 24 h day using the formulation developed in Section 3. Finally, we present an economic analysis of the optimal operation strategy.

4.1. Demand and environment modeling

In this section, the models for energy demand and load profiles are presented. Moreover, a thorough discussion on the electricity tariffs used to define the cost structure is included.

4.1.1. Energy demand and load profiles

For the entire year of 2004, the U.S. Department of Energy published the demand profiles of 16 commercial and 3 residential reference buildings, separated by source (electricity, gas) and consumption type (e.g., lights, facility, heating, cooling) [63,64]. Based on the available data, the effectiveness of employing a MGT as a CHP unit is considered for four different buildings:

1. **A full service restaurant**: area of 511 m^2 on one floor level, on which the commercial medium electricity tariff applies.
2. **A large hotel**: area of 11,345 m^2 over 6 floor levels, on which the commercial tall electricity tariff applies.
3. **A small hotel**: area of 4013 m^2, over 4 floor levels, on which commercial medium electricity tariff applies.

4. **A residential building with high load**: a neighborhood consisting of 20 apartment buildings, on which the residential electricity tariff applies.

In the scope of this work, towards simplicity, the demand is categorized as general electrical power and heat (cooling is related to heat through the absorption chiller coefficient of performance). A histogram of the annual electricity load profiles of the reference buildings listed above is given in Fig. 9(a). The red dashed line marks the maximum electricity output that can be generated by the CHP unit considered in this investigation. Similarly, heat load curves are presented in Fig. 9(b), where the two horizontal red lines show the minimum (0% bypassing) and maximum (80% bypassing) heat production at maximal electricity output. The yearly hours portrayed are not consecutive, but rather a representation of frequency for a demand level above the designated value. It can be seen that for larger buildings (such as a large hotel), the maximum electrical output of a single unit is not sufficient to ever meet the entire demand, whereas the heat output is at times only partially fulfilled by the CHP. Contrasting this to the case of the restaurant, the heat and electrical capacity of the MGT consistently surpasses the need. For the other buildings types, the heat and electricity supplied by the MGT should be determined according to time-varying demand level and the associated cost with respect to the utility.

4.1.2. Electricity and heat tariffs

In general, many different electricity tariffs exist; they reward certain behavior while penalizing divergent conduct. In this work, aggregation of the electricity tariffs are modeled according to the framework proposed in [65]. As described in [66,67], the tariffs comprise three cost components: fixed costs (FC), fixed pricing of energy (FPE), and demand charging (DC). We denote by $g(\Delta P(t))$ the function that defines the cost of electricity,

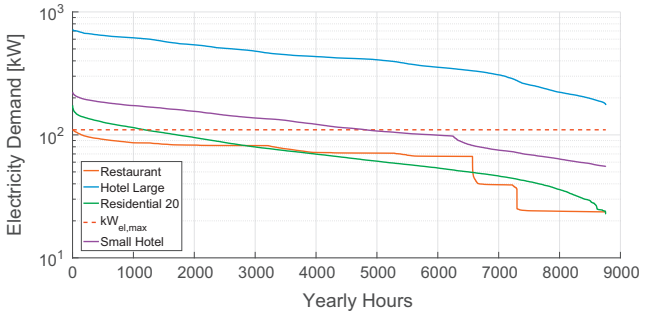

(a) Power demand histogram.

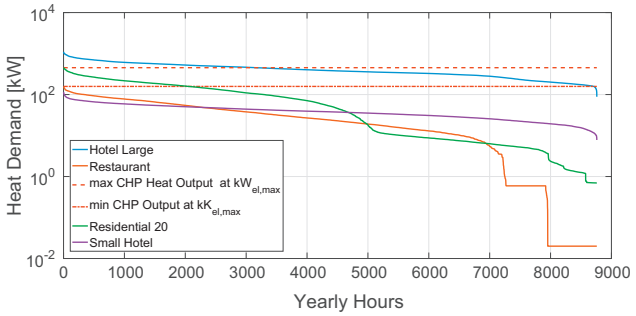

(b) Heat demand histogram.

Fig. 9. Histogram of annually demand profiles for different microgrid consumers. Output limitations of the CHP unit are highlighted.

$$g(\Delta P(t)) = \begin{cases} A \cdot \Delta T \cdot \Delta P(t) + B + C, & \Delta P(t) \geqslant 0 \\ A \cdot \Delta T \cdot \Delta P(t), & \Delta P(t) < 0 \end{cases}, \tag{22}$$

where

$$\Delta P(t) = P(t) - P_{GT}(x_{GT}(t))$$

and ΔT is the time step increment (in seconds) we use to schedule the MGT operation. In (22), A represents the (linear) energy charge (in \$/kW h), B the demand charge (in \$), and C is service and metering charge (in \$) - calculated per day of utilization.

The demand charge, B, is the cost associated with providing service during peak demand periods. It is used to penalize the power consumption in commercial buildings based on the highest average kW maintained during any 15-min interval within the billing cycle [68]. The charge B is divided into two different components, the peak demand charge (PDC), and the intermediate demand charge (IDC), and is defined as,

$$B = \begin{cases} \text{summer} \\ \frac{1}{30}\left(\text{PDC} \cdot \max_{t \in t_{\text{peak}}}(P(t)) + \text{IDC} \cdot \max_{t \in t_{\text{int}}}(P(t))\right) \\ \text{winter} \\ \frac{1}{30}\text{IDC} \cdot \max_{t \in t_{\text{int}}}(P(t)) \end{cases}, \tag{23}$$

where t_{peak} represents the peak hours and t_{int} the intermediate hours (see Table 3). Usually the billing cycle is a full month, but in this study, its contribution to a single day is considered; therefore, the value obtained is divided by 30 (average month duration) to yield the daily contribution to the cost.

As discussed in Section 3, a cost must be assigned to each transition edge modeling the operation of the MGT in the economic dispatch problem. Based on the tariff model (22), only the linear energy charge, A, is used to compute the cost of an edge in (21). For the purpose of this study, we apply the fixed usage costs B and C *a posteriori* to provide a more accurate economic analysis.

The rates A, B, C, of each building type are different and vary according to the time of the day. In this work, pricing data from PSEG Long Island New York is used [66,67], summarized in Table 2. The pricing is based on Time-of-Use and fixed costs for all buildings (A and C in (22)), in addition to demand charge applied only to commercial medium and tall buildings (B in (22)). Within this structure, the cost of time-of-use and demand charges are regulated at different time intervals. The *peak hours* refer to time periods with high load on the grid, whereas low load hours (typically during the evenings) are denoted as *off-peak*; and hours between these times with moderate demand, are evaluated on an *intermediate* pricing level. The exact definition of peak, intermediate, and off peak hours vary depending on the building type and the season. Splitting the year into two seasons (summer/winter), *summer* is defined to be the time period between June 1st and September 30th. A complete definition of these peak, intermediate, and off peak intervals is given in Table 3. Therein, it can be seen that the peak pricing only applies to the summer period.

In addition to electricity, the energy source for heat/chill can also be obtained from the utility to achieve energy balance between the demand and supply. As most consumers use a boiler to satisfy their heat demand, we model the heating cost with the price of natural gas. The boiler can be modeled by the grouping of a combustor with a heat recovery unit, described by (6) and (14) respectively. Combining the two previous equations, the heating power of the boiler can be related to the fuel flow rate as,

$$\frac{P_{heat}}{\dot{m}_f} = \eta_{HRU}(AFR + 1)\left(\frac{\dot{Q}_r \eta_b + AFR \cdot h_{amb}}{AFR + 1} - h_{100^\circ\text{C}}\right), \tag{24}$$

where h_{amb} is the specific enthalpy of ambient temperature air at the combustor inlet, and $h_{100^\circ\text{C}}$ represents the specific enthalpy of

Table 2
Electricity tariff rates.

		Off peak	Intermediate	Peak
Commercial medium (restaurant, small hotel)	*A*	$/kW h 0.0273	$/kW h 0.0412	$/kW h 0.0444
	PDC/IDC	–	$/kW 3.9	$/kW 45.48
	C		$ 1.68	
Commercial tall (large hotel)	*A*	$/kW h 0.0291	$/kW h 0.0435	$/kW h 0.0543
	PDC/IDC	–	$/kW 5.34	$/kW 22.44
	C		$ 10.16	
Residential (residential neighborhood)	*A*	$/kW h 0.0442	$/kW h 0.0866	$/kW h 0.2461
	PDC/IDC	–	–	–
	C		$ 1.65	

Table 3
Definition of off peak, intermediate and peak periods for both seasons.

		Summer	Winter
Commercial medium	Off peak	23:00–07:00	23:00–07:00
	Intermediate	07:00–12:00 & 20:00–23:00	07:00–23:00
	Peak	12:00–20:00	–
Commercial tall	Off peak	00:00–07:00	00:00–07:00
	Intermediate	07:00–10:00 & 22:00–24:00	07:00–24:00
	Peak	10:00–22:00	–
Residential	Off peak	20:00–10:00	20:00–10:00
	Intermediate	–	10:00–20:00
	Peak	10:00–20:00	–

exhaust gasses (considered to be at 100 °C). The air to fuel ratio (AFR) is assumed to be constant and for natural gas $AFR = 17.2 \cdot 1.2 = 20.64$, where 17.2 is the stoichiometric ratio for methane-air mixture and the factor 1.2 is associated with the typical 20% lean burn.

For the chill production, buildings typically employ either conventional electric motor-powered chillers or gas-fired absorption cycle systems. The latter reduces the demand on the grid which can help alleviate the high electric costs in the summer when the peak hour charges apply. In order to provide an impartial assessment to the value of the MGT with respect to the utility, the consumers are assumed to be using absorption chillers to satisfy their cooling demands. This implies that the chill demand can be related to the heat demand by the absorption chiller's COP factor (0.7). Thereby, the cost of purchasing heating and cooling from the utility can be lumped into the price of natural gas.

4.1.3. Net metering

As the production capacity of the micro CHP unit is finite and predetermined, the energy balance between the local demand, the CHP output, and the utility commitment must be met, according to (17)-(18). Thus, depending on factors including the demand level and cost of fuel, power can be either bought from or sold to the utility.

One of the common approaches for regulating and accounting excess electricity (i.e., the difference between generated power and the demand) is known as *net metering* [69]. The bi-directional electricity flow in and out of the grid is typically accounted at the same tariff rate. Hence, net metering values excess power at retail cost. This is captured in (22) such that when the generation cost is negative ($\Delta P(t) < 0$) and the electricity is sold back to the grid.

As heat is not a directly tradable quantity, there is no mechanism equivalent to net metering for the transfer of thermal energy. Thus, any excess heat generated by the CHP is simply released to the environment.

4.2. Economic dispatch

For the case studies considered in this work, we take $\mathrm{s} = 9$ speed levels for the turbine, $\mathrm{v} = 5$ valve settings (from 0% to 80 %), and a time step of $\Delta T = 15sec$. Thus, at each time step, the MGT can assume 1 of $\mathrm{sv} + 1 = 46$ states, which includes one off-line state. We also note that for this time-step, ramp-rate constraints are not relevant as the MGT dynamics are much faster [14]. For a 24 h horizon, the resulting shortest path graph contains $2,649,262$ nodes and $2,003,946$ edges. The shortest path problem was solved using MATLAB's native shortest path solver on an Intel Core i7 3.60 GHz processor with 32 GB RAM PC, and the running time was on the order of seconds.

In the examples to follow, we consider a fixed gas price of $\$7.74/1000\ \mathrm{ft}^3$. This value is the reference cost on October 2015 [70], and it can be related to cost of fuel mass flow rate through the density of methane, $\rho_{CH_4} = 0.68 kg/m^3$.

In order to demonstrate the typical operational behavior of the system, the economic dispatch problem is solved over three reference days, which represent typical seasonal variations: a winter day (January 10th), a mid-season day (April 10th), and a summer day (July 10th). Each of these days contribute to the aggregate demand data presented in Fig. 9. Given that electrical companies usually define two different rating periods [66,67], *summer* (June 1st - September 30th) and *winter* (October 1st - May 31st), these exemplary days are sufficient to accurately depict the trends for the whole year. Furthermore, the actual demand data is only available in an hourly basis. In order to form a more realistic dynamic demand profile, the data is smoothed with a moving average filter (with a time window of 5 min) to ensure more gradual transitions of the demand.

We also note that we do not impose any constraints on the starting or ending state of the MGT in our 24-h economic dispatch. Furthermore, the optimization may chose any start or end state without penalty. This is motivated by the fact that the demand profiles do not vary significantly within a given season.

4.2.1. Full service restaurant

Figs. 10(a)–(f) show the solution of the economic dispatch problem (20) for a full service restaurant during each of the three reference days. As expected, the sum of the utility and the MGT commitments satisfy the instantaneous heat and electricity needs on all days. The power demand profiles roughly have the same order of magnitude in the three considered days, but the heat demand profile in the winter day (Fig. 10(d)) is significantly higher. Furthermore, although the restaurant's entire heat/electricity demands can be fulfilled by the MGT alone (see Fig. 9), it can be seen in Figs. 10(a)–(f) that this is not the most cost effective solution. During the entire winter day, the optimization sets the bypass valve at a constant 0%, while the fluctuation in the power and heat are associated with MGT speed variations.

On most of the winter day hours (05–01 h), the heat demand is mainly provided by the CHP, regardless of intermediate and off-peak tariff rates. Thus, the MGT is operated on a *heat driven* basis. Consequently, the ensuing CHP power is an artifact of the optimization, and the residual difference between the electricity production and demand is either supplied to or bought by the utility. For example, in the first hour of operation (24–01 h), the heat demand (126 kW) is primarily accommodated by the CHP unit, and only a small amount is purchased from the utility (10 kW), whereas the CHP power production (80 kW) is significantly higher than the electricity demand (39 kW). If the electricity and heat demand would have been met entirely from the utility, the cost would be $5.478 (considering the off-peak electrical charge and the utility heat production based on the natural gas pricing). Alternatively for the optimal CHP economic dispatch, the total operational cost is $5.702. However, as the electricity production exceeds the demand, the surplus is sold back to the grid, resulting in a profit of $1.119. On the other hand, the CHP heat production does not fulfill the entire demand, requiring in an additional utility cost of $0.398. In total, the net gain in operating the CHP unit during this hour amounts to $0.497.

From 01 h until 05 h (which is during the off-peak tariff period), the MGT is operated at an electricity and heat production level above the demand. This is a mode of operation which is *maintenance-cost driven*. The comparative advantage of the CHP over the utility should be in time intervals of higher heat demand or increased utility electricity pricing. However, in this off-peak time period, the operational state of the MGT is optimized to minimize losses. There is a direct low cycle fatigue associated cost of each shutdown and startup ($3.75), in addition to the fuel burned during the 3 and 2 min transitional time periods from on-to-off and off-to-on states.

Therefore, in this circumstance, the optimal state of the MGT is to continue its operation in the minimum possible electricity and heat production levels, 30 kW and 57 kW respectively. It simply happens to be that the electricity produced is above the power demand level.

For spring and summer days, it is not viable to operate the CHP unit at all. As the heat demand (up to 40 kW) is significantly lower than in the typical winter day (roughly 1/3), the largely unchanged electricity consumption (up to 105 kW) constitutes the primary energy cost. Both at the peak hours of the summer and at the off-peak hours of the same day (e.g., between 24 h and 01 h), the price of buying the necessary energy from the utility is cheaper than operating the MGT (e.g., $5.8114 with respect to $8.0298 between 15 h and 16 h and $0.6793 with respect to $2.8941 between 24 h and 01 h respectively). It can be seen that when the heat demand is low, the CHP unit vastly looses its comparative

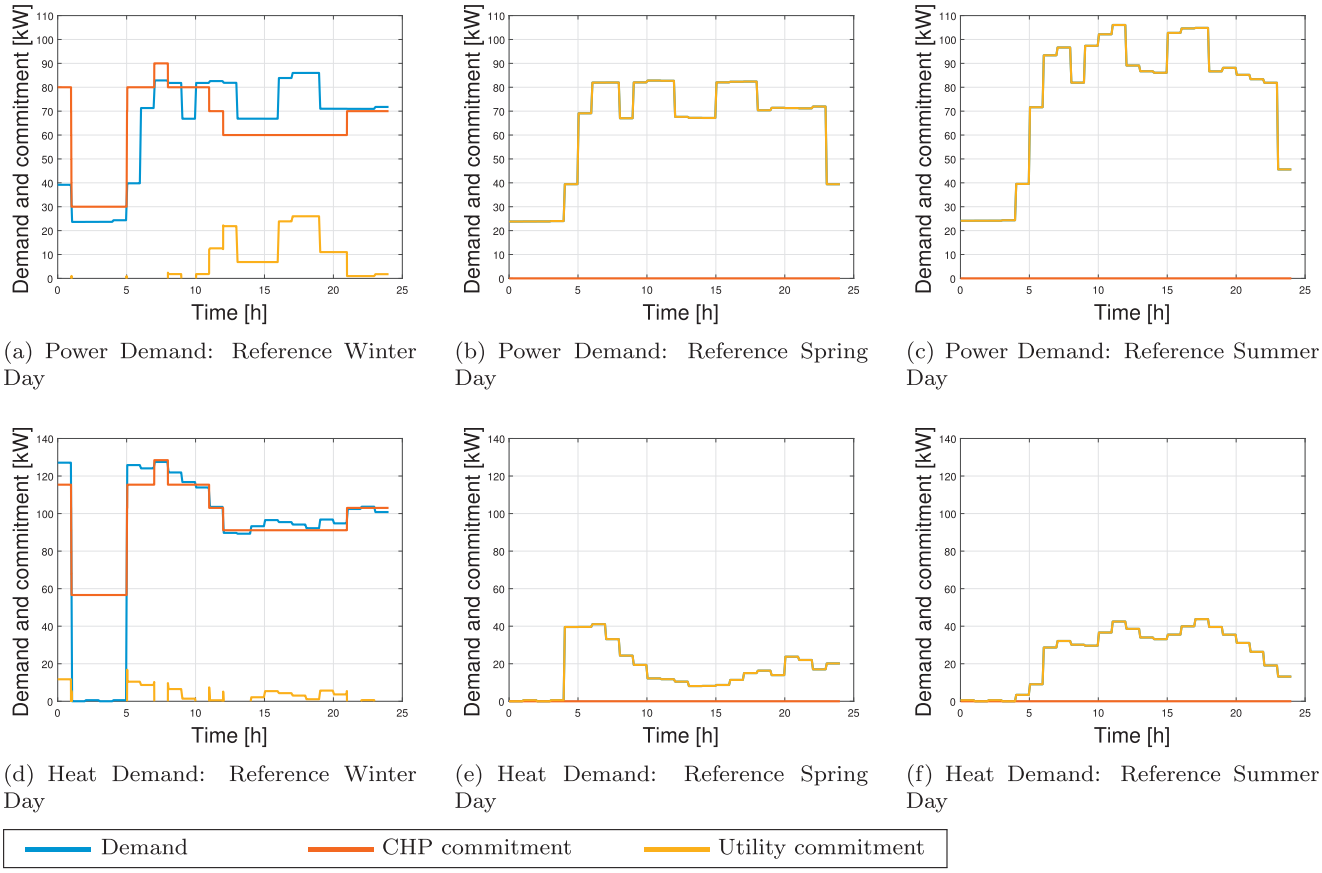

(a) Power Demand: Reference Winter Day

(b) Power Demand: Reference Spring Day

(c) Power Demand: Reference Summer Day

(d) Heat Demand: Reference Winter Day

(e) Heat Demand: Reference Spring Day

(f) Heat Demand: Reference Summer Day

Fig. 10. Heat and power demand of the full service restaurant and its economic dispatch solution for the seasonal reference days in winter, spring and summer.

advantage over the utility. This is also a maintenance-cost driven solution. If there was no penalty associated with cycling the MGT, there would be bursts of operation during peak tariff periods especially in the summer.

Remark 1. It is important to note that the resolution of the model discretization influences the solution of the economic dispatch problem. For example, in the heat driven scenario of the winter day, the MGT heat generation at 0% bypass valve setting is inferior to the heat demand. The valve position of the model (20%) would produce excess heat, which would have to be dumped. In order to be competitive with the utility electricity prices, the bypass level is maintained at 0%. In reality, there exists an optimal bypass valve setting between 0–20%, which would fully satisfy the heat demand with the MGT operation alone. As the complexity of the transition graphs grows exponentially with the number of states, this level of refinement will lead to computational problems and are thus beyond the scope of this investigation.

4.2.2. Large hotel

A similar optimization is conducted for the demand profiles of the large hotel and the results are depicted in Figs. 11(a)–(f). For the entire yearly hours, the power demand is consistently greater than the maximum unit capacity (110 kW) and the heat demand is above the minimum MGT output (57 kW) (see Fig. 9). Moreover, in about one third of the yearly hours, the heat load of the large hotel is higher than the maximal CHP heat output. Therefore, for all reference cases, the heat and power demands are satisfied by the contributions of both the MGT and the utility.

For all days in between 07 h and 24 h (in the intermediate tariff period and peak tariff period during the summer), the MGT operates consistently at the highest electricity production level of 110 kW, while the supplied CHP heat is 193 kW. Operating as a base load system, the MGT shaft speed is 100% with bypass setting of 20%. However, in the off-peak tariff period (24–07 h), the cost of purchasing electricity from the utility drops, and the equilibrium between the CHP unit's electrical efficiency and the network supply price changes. The new energy equilibrium operates at a shaft speed of 89% and a valve setting of 0%, not explicitly shown in the figure. With the decreasing comparative advantage of the CHP, the optimal solution is in a more thermodynamically efficient MGT state, generating 80 kW and 144 kW of electricity and heat respectively, while the remainder is bought from the utility. Despite the heat and electricity demand which exceeds the CHP unit capacity, the optimal solution is demonstrated to be in partial load operation. Overall for this building type, the CHP operates as a base load system for intermediate and peak tariff periods. This a combination of *electricity driven* and *heat driven* modes of operation.

Remark 2. Considering the resultant consistent reduction in the electricity purchase from the utility for all hours of every reference day, it is expected that demand peaks and the associated charges will be lowered. This will yield considerable savings; nevertheless, the optimization does not directly consider this factor.

4.2.3. Small hotel

Another considered consumer is a typical small hotel, with a year long power demand consistently above 110*kW* (beyond the capacity of the MGT), and a heat demand below 100 kW. Like the full service restaurant and the large hotel, this building is rated with a commercial tariff. In this scenario, the optimal operation strategy for winter (Figs. 12(a), (d)) and summer (Figs. 12(c), (f))

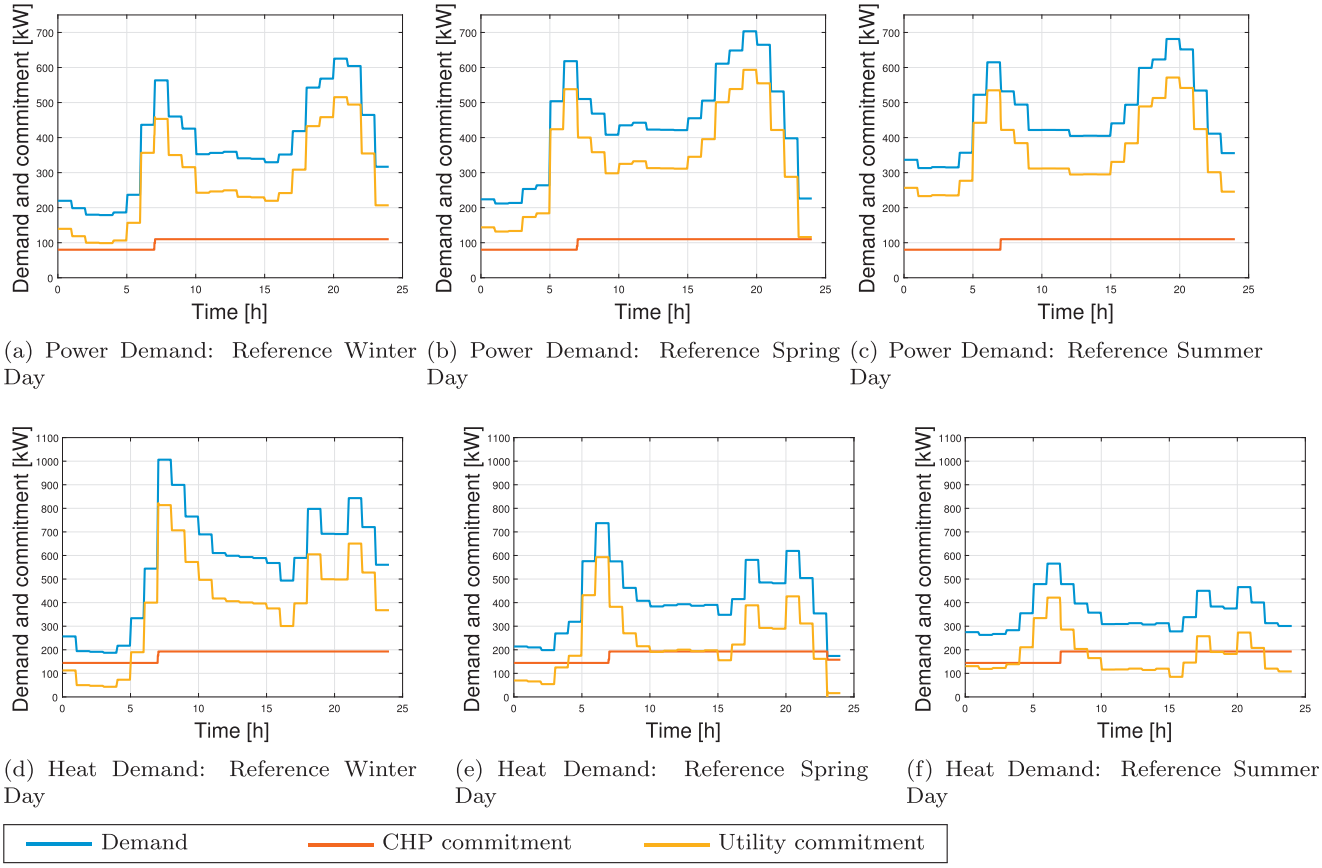

(a) Power Demand: Reference Winter Day (b) Power Demand: Reference Spring Day (c) Power Demand: Reference Summer Day

(d) Heat Demand: Reference Winter Day (e) Heat Demand: Reference Spring Day (f) Heat Demand: Reference Summer Day

Fig. 11. Heat and power demand of the large hotel and its economic dispatch solution for the seasonal reference days in winter, spring and summer.

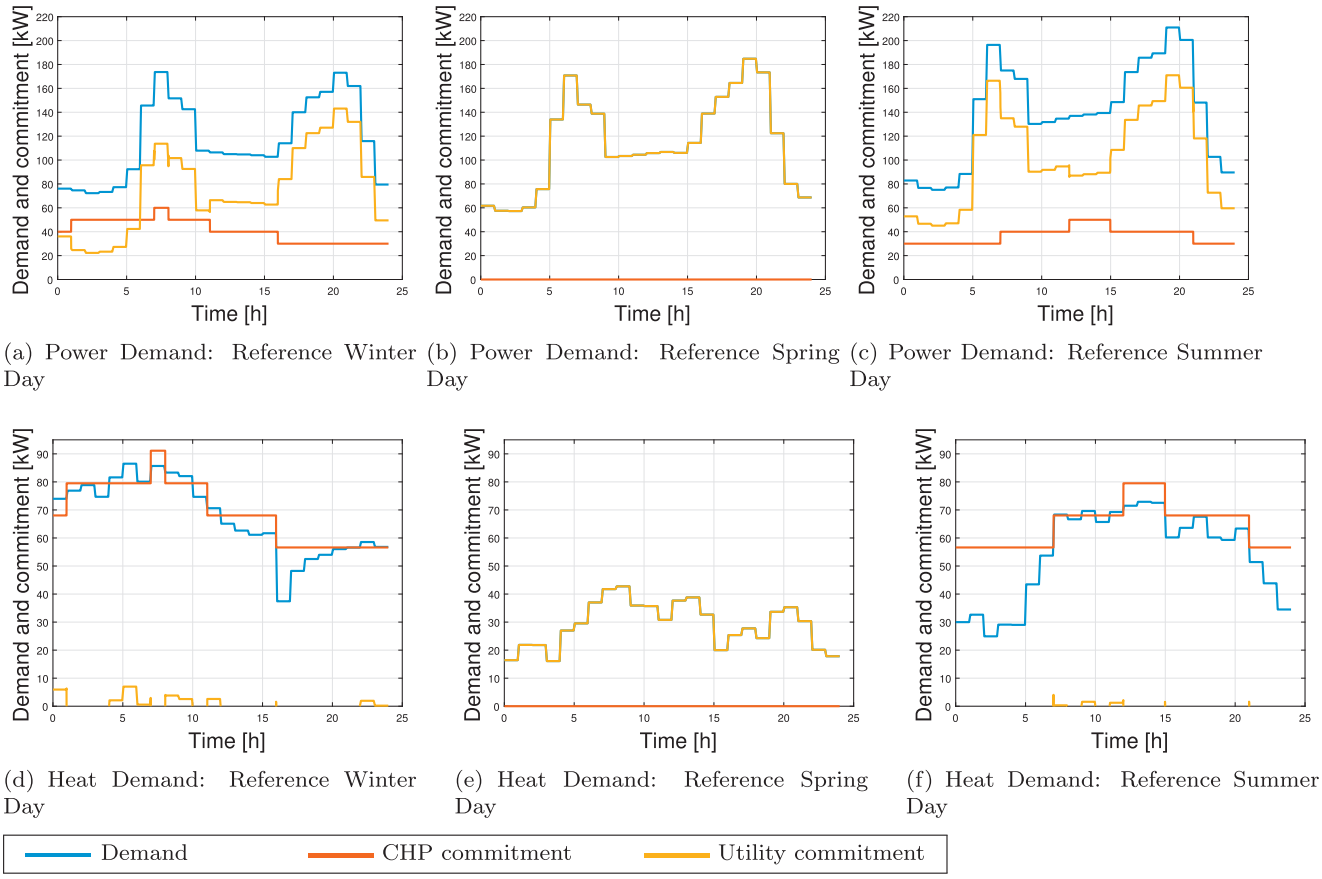

(a) Power Demand: Reference Winter Day (b) Power Demand: Reference Spring Day (c) Power Demand: Reference Summer Day

(d) Heat Demand: Reference Winter Day (e) Heat Demand: Reference Spring Day (f) Heat Demand: Reference Summer Day

Fig. 12. Heat and power demand of the small hotel and its economic dispatch solution for the seasonal reference days in winter, spring and summer.

is similar. Operating the unit at a low power commitment level, the heat demand is supplied at a competitive unit efficiency (0% bypass). Clearly the behavior is heat driven, except in the off-peak hours of the summer, when it is more economical to continue operation at minimum production level instead of shutting down (maintenance driven). In contrast to summer and winter, the spring day exhibits a low heat demand profile, while the power demand is at a comparable level with other seasons (Figs. 12(b), (e)). The optimization finds that it is not profitable to operate the unit, and therefore the MGT stays off the whole day.

4.2.4. Residential neighborhood

For the residential neighborhood scenario, the solution of the CHP unit economic dispatch are presented in Figs. 13(a)–(f). On the reference winter day, the CHP unit operates at constant heat (193 kW) and maximum electricity production (110 kW). Between 17 h and 22 h, when the power demand surpasses the MGT capacity, additional electricity is bought from the utility. In all other time intervals, the excess electricity is sold to the grid according to net metering procedure. It is interesting to note that the heat production is kept at a constant level (at 20% bypass) throughout the day, and it is more economical to purchase additional heat from the utility when needed. This is in part associated with the relatively course bypass valve grid employed in the optimization (see Remark 1).

During the typical spring day, the MGT unit behavior presents a unique operational schedule which is *revenue driven*. In the intermediate tariff hours of the day (10–20 h), the CHP unit operates at an electricity and heat production level significantly beyond the consumer demand, selling all the excess electricity to the grid while dumping the excess heat to the atmosphere (see Figs. 13(b) and (e)). Therefore, the optimal solution is to take advantage of the higher electricity rates during this period to increase revenue. In fact, in order to increase the electrical efficiency, the bypass valve is set at 0% and the associated heat commitment level is the lowest possible for the chosen speed setting. In this particular circumstance, the MGT can clearly produce electricity at a lower per unit cost than the utility. In the late evening from 20 h to 24 h, when the utility costs are low, the CHP operates at its lowest possible power and heat state instead of shutting down (maintenance driven). For the same day, in the off-peak tariff hours (24–10 h), the CHP unit supplies the entire heat demand at 0% bypass and varying speed levels (heat driven behavior). If available, the ensuing excess electricity is sold back to the grid.

During the summer day, the electricity is at peak rate between 10 h and 20 h, which increases the economic advantage of production by the MGT. In fact, between 10 h and 11 h, the unit produces 110*kW* electricity at 0% bypass (greater than the demand) and sells the surplus back to the grid (revenue driven). From 12 h to 20 h, the power demand exceeds the capacity of the MGT, and the additional requirements are supplied by the utility. However, this time period is not entirely electricity driven. Between 16 h and 17 h, with the increasing heat demand, the bypass valve position is adjusted to 20% in order to produce more heat at the same electricity production rate (100% speed). Hence, the optimization finds economic advantage in producing heat through the MGT at the expense of augmented fuel consumption. In the off-peak hours of 20–24 h and 07–10 h, the trends are heat driven due to lowered price of electricity. Once again, in the early hours of the day between 24 h and 07 h, the MGT operates in its minimum electricity and heat production state, instead of shutting down (maintenance driven). In this time period, it is more economical to fulfill the additional electricity demand from the network.

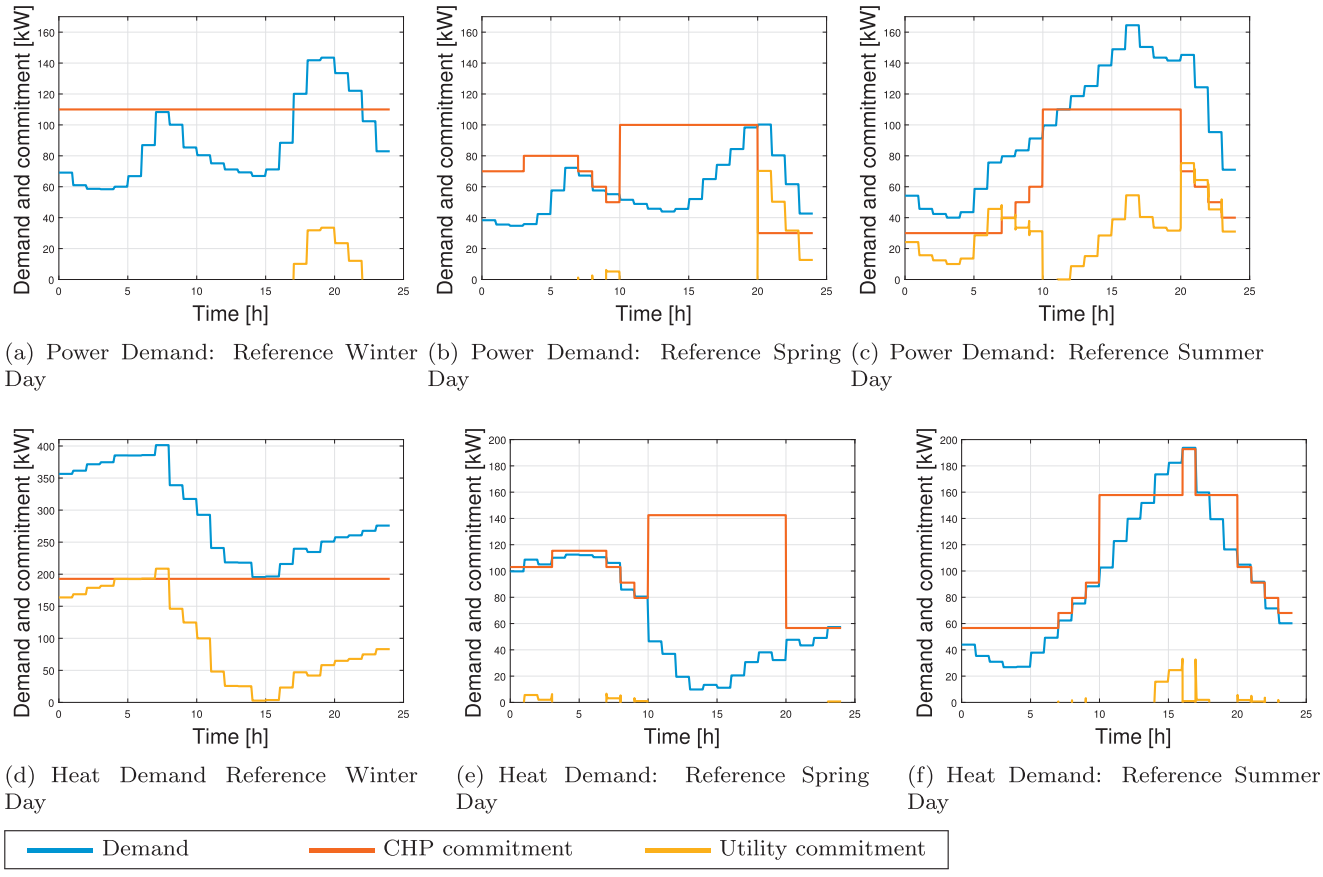

(a) Power Demand: Reference Winter Day (b) Power Demand: Reference Spring Day (c) Power Demand: Reference Summer Day

(d) Heat Demand Reference Winter Day (e) Heat Demand: Reference Spring Day (f) Heat Demand: Reference Summer Day

Fig. 13. Heat and power demand of the residential community and its economic dispatch solution for the seasonal reference days in winter, spring and summer.

Throughout the various seasons and times of day, the residential neighborhood presents differing optimal commitment trends associated with heat, electricity, revenue, and maintenance-cost driven operation. In contrast to other consumers of energy, the increased diversity in the neighborhood's economic dispatch mode is heavily based on the variations in the ratio between the power to heat demand, which fluctuates between 0.2–6. In contrast, the heat to power demand ratio of the restaurant varies between roughly 0–1.5 throughout the year. This increased range of this ratio has strong influence on the optimization strategies.

4.3. A comparison against base-load operation

Integrating an MGT as a base-load unit typically involves comparing the cost of purchasing electricity from the utility against the cost of local generation. The graph in Fig. 14 shows the linear tariff charge (the coefficient A in (22)) for each building type and for different times of day (peak, intermediate, and off-peak). The dashed horizontal lines represent the cost of electricity generation for the MGT at full speed and 0% bypass for the October 2015 reference fuel cost of \$7.74/1000 ft^3 along with moderate deviations from that period (\$8.85/1000 ft^3 and \$6.80/1000 ft^3) [70]. This chart shows the scenarios when it is economically viable to operate in a revenue and/or electricity driven mode. Indeed, it is not economical to operate commercial medium buildings in electricity driven modes at any time. This leads to a heat driven and/or maintenance driven operation, as seen in the case study for the small hotel and restaurant. In contrast, for commercial tall buildings (large hotel), it is advantageous to operate in an electrical driven mode during peak periods. Similarly, for residential buildings, both electricity driven and revenue driven modes are economically preferable during intermediate and peak periods, as indicated by the significant cost difference between the utility and the MGT.

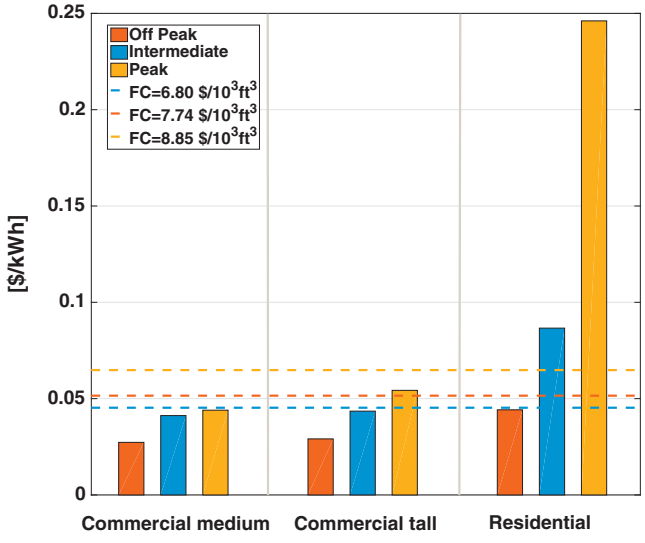

Fig. 14. Cost comparison of purchasing electricity from the utility against using the MGT as a base-load unit.

4.4. Economic analysis

To effectively demonstrate the economic viability of integrating the MGT, Table 4 summarizes the total savings when the natural

Table 4
Absolute daily savings, for all buildings, days and fuel cost combinations ($).

Fuel cost ($/1000 ft^3)	Full service restaurant			Small hotel			Residential			Large hotel		
	7.74	8.85	6.80	7.74	8.85	6.80	7.74	8.85	6.80	7.74	8.85	6.80
Winter day	22.66	16.82	27.76	12.00	8.07	16.86	97.17	88.40	105.21	58.78	49.62	66.03
Spring day	0.00	0.00	0.00	0.00	0.00	0.00	37.85	26.90	48.58	58.74	49.60	66.00
Summer day	0.00	0.00	0.00	67.40	0.00	87.26	241.32	233.42	248.27	150.27	141.97	159.10

Table 5
Daily demand charging savings, for all buildings, days and fuel cost combinations ($).

Fuel cost ($/1000 ft^3)		Full service restaurant			Small hotel			Residential			Large hotel		
		7.74	8.85	6.80	7.74	8.85	6.80	7.74	8.85	6.80	7.74	8.85	6.80
Winter day	Peak	0.00	0.00	0.00	0.00	0.00	0.00	0.00	0.00	0.00	0.00	0.00	0.00
	Intermediate	7.80	7.80	7.80	3.98	3.98	5.28	0.00	0.00	0.00	19.58	17.80	19.58
Spring day	Peak	0.00	0.00	0.00	0.00	0.00	0.00	0.00	0.00	0.00	0.00	0.00	0.00
	Intermediate	0.00	0.00	0.00	0.00	0.00	0.00	0.00	0.00	0.00	19.58	17.80	19.58
Summer day	Peak	0.00	0.00	0.00	60.64	0.00	75.80	0.00	0.00	0.00	82.28	82.28	74.80
	Intermediate	0.00	0.00	0.00	5.20	0.00	5.88	0.00	0.00	0.00	19.58	14.25	19.58

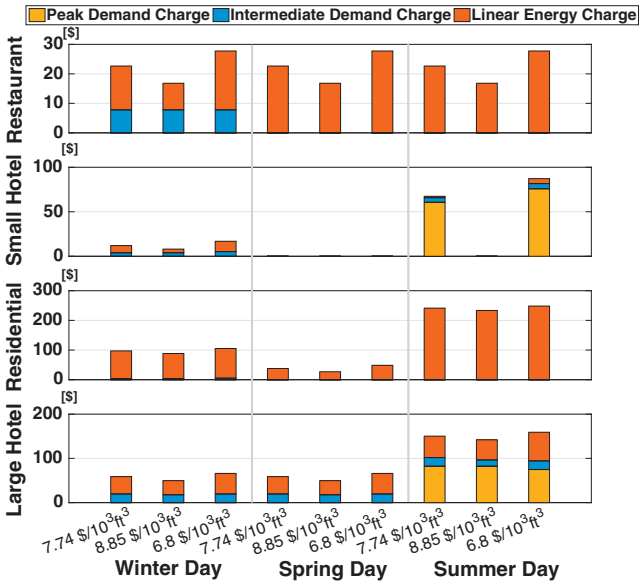

Fig. 15. Distribution of cost savings resulting from the case studies.

gas price moderately deviates from the October 2015 reference of fuel cost 1 = $7.74/1000 ft^3 to fuel cost 2 = $8.85/1000 ft^3 and fuel cost 3 = $6.80/1000 ft^3 [70]. The results are aggregated by day (Summer, Spring/Autumn, Winter) and building types. If the savings are listed as zero, it is not economically beneficial to operate the CHP unit. To facilitate the analysis, the data is further broken down to show the demand charge savings, Table 5 (which are divided by 30 as the usual billing period is one month).

For the commercial tall and medium buildings, there are savings resulting from fixed pricing of electricity and demand charge reduction (Table 5). The latter is associated with operating the unit at a nearly constant commitment level that decreases the peak loads met by the utility. For these reasons, in the large hotel example, using a single CHP unit is especially advantageous (Table 4), however insufficient in terms of meeting demand. Therefore, a bank of CHP units may be more suitable to accommodate the energy needs. In general for all commercial buildings, increasing the fuel price leads to a decrease in savings. This is most clearly demonstrated in the small hotel, where increasing the fuel price renders the unit economically inoperable.

The largest savings are observed for the residential neighborhood (Table 4), despite the tariff which excludes demand charges (hence, the corresponding entries in Table 5 are null). All the savings stem from the fixed pricing of energy and revenue generation.

The savings data presented in Tables 4 and 5 are also visualized in Fig. 15. The chart shows the saving contribution due to the linear energy charges (determined by the coefficient A in (22)), and the peak and intermediate demand charges (the coefficient B in (22)). It is important to recall that the demand charge savings are a byproduct to the economic dispatch solution, which are computed *a posteriori*. The optimization does not actually attempt to minimize the demand charges. Nevertheless, it is remarkable that during the summer days, the main savings for both the small and large hotels are due to reduction of the peak and intermediate demand charges. Therefore, it would be of interest for future work to consider strategies that attempt to minimize the peak demand.

5. Conclusion

A comprehensive micro-gas turbine model was established for the purpose of optimizing the operational behavior of a CHP unit in a smart-grid environment. Real demand profiles and existing electricity tariffs were used to an accurate optimization model for solving the economic dispatch problem of an MGT unit under CHP operation. The unit commitment problem was then solved for four different typical consumers on representative days from all seasons. Of main interest is the observation that the optimal solution results in four distinct economically driven MGT operation modes: electricity driven, heat driven, maintenance cost driven, and revenue driven. For example, the power and heat demand of the large hotel exceeds the production capacity of the MGT, however the optimal solution shows at times partial commitment from the CHP unit, which is a combination of an electricity driven and heat driven behavior. On the other hand, for both the restaurant and the small hotel, the MGT commitment level is heat driven due to more competitive cost of energy generation with respect to the demand profile. In off-peak hours when the utility tariff is low, the schedule is maintenance driven to avoid cycle costs, leading to either a minimal commitment level, or completely off-line days. The residential neighborhood demonstrated heat and maintenance cost driven modes, in addition to a revenue driven operation aimed at generating excess electricity for profit. This diversity of operation stems from the large range of power to heat demand

ratios of this building. In all the case studies, the integration of a micro-gas turbine as a CHP unit in a smart grid setting leads to significant economic benefits.

Acknowledgment

The authors acknowledge the financial support of Technion-Israel Institute of Technology, Minerva Research Center (Max Planck Society Contract AZ5746940764), the Grand Technion Energy Program (GTEP Contract 1013145) and the IAESTE Portugal program.

References

[1] Criqui P. Prospective outlook on long-term energy systems: EUR 17358 EN, Bruselas; 1996.
[2] Eu energy in figures: statistical pocketbook 2015; 2015.
[3] U.S. Energy Information Administration. Annual energy outlook 2015. <http://www.eia.gov/forecasts/aeo/>.
[4] EU energy, transport and GHG emissions: trends to 2050 – reference scenario 2013; 2014.
[5] Pilavachi PA. Mini- and micro-gas turbines for combined heat and power. Appl Therm Eng 2002;22(18):2003–14.
[6] Peirs J, Waumans T, Vleugels P, Al-Bender F, Stevens T, Verstraete T, et al. Micropower generation with microgasturbines: a challenge. Proc Inst Mech Eng, Part C: J Mech Eng Sci 2007;221(4):489–500.
[7] Lymberopoulos N. Microturbines and their application in bio-energy: EESD contract no: Nne5-pta-2002-003/1; 2004.
[8] Gu W, Wu Z, Bo R, Liu W, Zhou G, Chen W, et al. Modeling, planning and optimal energy management of combined cooling, heating and power microgrid: a review. Int J Electr Power Energy Syst 2014;54:26–37.
[9] Liu M, Shi Y, Fang F. Combined cooling, heating and power systems: a survey. Renew Sustain Energy Rev 2014;35:1–22.
[10] Cho H, Luck R, Eksioglu SD, Chamra LM. Cost-optimized real-time operation of CHP systems. Energy Build 2009;41(4):445–51.
[11] Logan Jr E. Handbook of turbomachinery. CRC Press; 2003.
[12] Giampaolo T. The gas turbine handbook: principles and practices. CRC Press; 2003.
[13] Walsh PP, Fletcher P. Gas turbine performance. John Wiley & Sons; 2004.
[14] Yinger RJ. Behavior of Capstone and Honeywell microturbine generators during load changes. Lawrence Berkeley National Laboratory (February) 2001:38.
[15] Camporeale SM, Ciliberti PD, Fortunato B, Torresi M, Pantaleo AM. Externally fired micro gas turbine and ORC bottoming cycle: optimal biomass/natural gas CHP configuration for residential energy demand. In: ASME Turbo Expo. pp. V003T06A020-V003T06A020.
[16] Ferreira AC, Nunes ML, Teixeira SF, ao CPL, Silva AM, Teixeira JC, et al. An economic perspective on the optimisation of a small-scale cogeneration system for the portuguese scenario. Energy 2012;45(1):436–44.
[17] Mongibello L, Bianco N, Caliano M, Graditi G. Influence of heat dumping on the operation of residential micro-chp systems. Appl Energy 2015;160:206–20.
[18] Pantaleo A, Camporeale S, Shah N. Thermo-economic assessment of externally fired micro-gas turbine fired by natural gas and biomass: applications in Italy. Energy Convers Manage 2013;75:202–13.
[19] Camporeale SM, Fortunato B, Torresi M, Turi F, Pantaleo AM, Pellerano A. Part load performance and operating strategies of a natural gasbiomass dual fueled microturbine for combined heat and power generation. J Eng Gas Turbines Power 2015;137(12):121401–14.
[20] Bracco S, Delfino F. A mathematical model for the dynamic simulation of low size cogeneration gas turbines within smart microgrids. Energy 2017;119:710–23.
[21] Galanti L, Massardo AF. Micro gas turbine thermodynamic and economic analysis up to 500 kwe size. Appl Energy 2011;88(12):4795–802.
[22] Al-Hinai A, Feliachi A. Dynamic model of a microturbine used as a distributed generator. In: IEEE proceedings of the thirty-fourth southeastern symposium on system theory. p. 209–13.
[23] Lasseter R. Dynamic models for micro-turbines and fuel cells. IEEE power engineering society summer meeting, vol. 2. p. 761–6.
[24] Hannett LN, Jee G, Fardanesh B. A governor/turbine model for a twin-shaft combustion turbine. IEEE Trans Power Syst 1995;10(1):133–40.
[25] Hannett L, Khan A. Combustion turbine dynamic model validation from tests. IEEE Trans Power Syst 1993;8(1):152–8.
[26] Badami M, Portoraro A. Simulation model and experimental validation of a CHP plant with micro gas turbine. In: Proceedings of the ASME: international mechanical engineering congress & exposition, Houston, TX. p. 1–12.
[27] Gopisetty S, Treffinger P. Generic combined heat and power (CHP) model for the concept phase of energy planning process. Energies 2016;10(1):11.
[28] Duan J, Sun L, Wang G, Wu F. Nonlinear modeling of regenerative cycle micro gas turbine. Energy 2015;91:168–75.
[29] Nikpey H, Assadi M, Breuhaus P. Development of an optimized artificial neural network model for combined heat and power micro gas turbines. Appl Energy 2013;108:137–48.
[30] Sellers JF, Daniele CJ. DYNGEN – a program for calculating steady-state and transient performance of turbojet and turbofan engines; April, 1975.
[31] Chiang H-WD, Hsu C-N, Lai A, Lin R. An investigation of steady and dynamic performance of a small turbojet engine. In: ASME Turbo Expo. p. 1097–104.
[32] Kim MJ, Kim JH, Kim TS. Program development and simulation of dynamic operation of micro gas turbines. Appl Therm Eng 2016;108:122–30.
[33] Henke M, Monz T, Aigner M. Introduction of a new numerical simulation tool to analyze micro gas turbine cycle dynamics. J Eng Gas Turbines Power 2017;139(April):0462601–09.
[34] Ansaldo Energia Homepage. <http://www.ansaldoenergia.it/>.
[35] Capstone Turbine Corporation Homepage. <http://www.capstoneturbine.com/>.
[36] Durr cleantechnology homepage. <http://www.durr-cleantechnology.com/>.
[37] La micro-cogenerazione a gas naturale: una nuova via del risparmio energetico: Sileo, m. <http://www.ambientediritto.it/dottrina/Politiche%20energetiche%20ambientali/politiche%20e.a/micro_cogenerazione_sileo.htm>.
[38] Ingersoll-Rand Energy Systems. Test and quality assurance plan – IR power works – 70 kW microturbine system, SRI/USEPA-GHG-QAP-21; 2002.
[39] Ingersoll-Rand Energy Systems. ETV joint verification statement, SRI/USEPA-VS-GHG-VR-21; 2003.
[40] Jones A. Npt-171 turbojet performance prediction method. Noel Penny Turbine Ltd., internal publication; 1983. p. 2–21.
[41] Hx cpt 95-9-0 gas turbine heat recuperator. <http://www.acte-sa.be/> (2015-03).
[42] Waste heat recovery: technology and opportunities in the U.S. industry. <http://www1.eere.energy.gov/manufacturing/intensiveprocesses/pdfs/waste_heat_recovery.pdf>.
[43] Kren C. Flue gas fired absorption chillers. Dissertation, München; 2006.
[44] Waste heat integration of electrical power generation provided by fuel cells. <http://epb.lbl.gov/thermal/waste.html>.
[45] Advanced Manufacturing Office. Use low-grade waste steam to power absorption chillers: energy tips: steam; 2012. <https://www1.eere.energy.gov/manufacturing/tech_assistance/pdfs/steam14_chillers.pdf>.
[46] Kadosh K, Cukurel B. Micro-turbojet to turbofan conversion via continuously variable transmission: thermodynamic performance study. J Eng Gas Turbines Power 2017;139(2):022603–13.
[47] Xia X, Elaiw AM. Optimal dynamic economic dispatch of generation: a review. Electric Power Syst Res 2010;80(8):975–86.
[48] Saravanan B, Das S, Sikri S, Kothari DP. A solution to the unit commitment problem-a review. Front Energy 2013;7(2):223–36.
[49] Elsayed WT, Hegazy YG, Bendary FM, El-Bages MS. A review on accuracy issues related to solving the non-convex economic dispatch problem. Electric Power Syst Res 2016;141:325–32.
[50] Farhat IA, El-Hawary ME. Optimization methods applied for solving the short-term hydrothermal coordination problem. Electric Power Syst Res 2009;79(9):1308–20.
[51] Yamin HY. Review on methods of generation scheduling in electric power systems. Electric Power Syst Res 2004;69(2–3):227–48.
[52] Padhy N. Unit commitment a bibliographical survey. IEEE Trans Power Syst 2004;19(2):1196–205.
[53] Travers DL, John Kaye R. Dynamic dispatch by constructive dynamic programming. IEEE Trans Power Syst 1998;13(1):72–8.
[54] Snyder WL, Powell HD, Rayburn JC. Dynamic programming approach to unit commitment. IEEE Trans Power Syst 1987;2(2):339–48.
[55] Thakur N, Titare LS. Determination of unit commitment problem using dynamic programming. Int J Novel Res Electr Mech Eng 2016;3(1):24–8.
[56] Bertsekas DP, Lauer GS, Sandell NR, Posbergh TA. Optimal short-term scheduling of large-scale power systems. IEEE Trans Autom Control 1983(AC 28 No. 1):1–11.
[57] Bertsekas DP. Dynamic programming and optimal control. Athena scientific optimization and computation series, 3rd ed., vol. 3. Belmont, Mass.: Athena Scientific; 2007.
[58] Bertsekas DP. Network optimization: continuous and discrete models (optimization, computation, and control). Athena Scientific; 1998.
[59] Zelazo D, Dai R, Mesbahi M. An energy management system for off-grid power systems. Energy Syst 2012;3(2):153–79.
[60] Cormen TH, Stein C, Rivest RL, Leiserson CE. Introduction to algorithms. 2nd ed. McGraw-Hill Higher Education; 2001.
[61] Kahn AB. Topological sorting of large networks. Commun ACM 1962;5(11):558–62.
[62] Majumdar S. Low-cycle fatigue and creep analysis of gas turbine engine components. J Aircraft 1975;12(4):376–82.
[63] Commercial Reference Buildings. <http://energy.gov/eere/buildings/commercial-reference-buildings>.
[64] Building characteristics for residential hourly load data: based on building america house simulation protocols; 2010. <http://en.openei.org/doe-opendata/dataset/eadfbd10-67a2-4f64-a394-3176c7b686c1/resource/cd6704ba-3f53-4632-8d08-c9597842fde3/download/buildingcharacteristicsforresidentialhourlyloaddata.pdf>.
[65] Beaudin M, Zareipour H. Home energy management systems: A review of modelling and complexity. Renew Sustain Energy Rev 2015;45:318–35.

[66] PSEG LINY. Tariff for electric service residential; 2016. <https://www.psegliny.com/files.cfm/rates_resi.pdf>.
[67] PSEG LINY. Tariff for electric service commercial; 2016.
[68] How to read your bill. <https://www.psegliny.com/page.cfm/Commercial/Account/MyBill/ReadBill> (2016-9).
[69] Sajjad IA, Manganelli M, Martirano L, Napoli R, Chicco G, Parise G. Net metering benefits for residential buildings: a case study in Italy. In: IEEE 15th international conference on environment and electrical engineering (EEEIC). p. 1647–52.
[70] U.S. Energy Information Administration. U.S. Natural Gas Prices; 2016. <https://www.eia.gov/dnav/ng/ng_pri_sum_dcu_nus_a.htm>.